

1-
DTIC
①

A Final Technical Report

from

CHARLES EVANS & ASSOCIATES
1670 South Amphlett Blvd., Suite #120
San Mateo, CA 94402
(415) 572-1601

DTIC
ELECTE
JAN 09 1986
S D

Development and Application of SIMS Characterization Techniques for the Study
of Impurities and Impurity Motion in (HgCd)Te and CdTe

sponsored by:

Defense Advanced Research Projects Agency (DOD)
ARPA Order #4606 DSO/ES

Under Contract #MDA903-82-C-0427 by Department of the Army,
Defense Supply Service-Washington,
Washington, DC 20310

Principal Investigator:

Charles A. Evans, Jr.
President

DISTRIBUTION STATEMENT A
Approved for public release
Distribution Unlimited

CLEARED

FOR OPEN PUBLICATION

Effective Date: November 1, 1983

Expiration Date: September 30, 1985

Reporting Period: November 1, 1983 - September 30, 1985

JAN 02 1986 21

DIRECTORATE FOR FREEDOM OF INFORMATION
AND SECURITY REVIEW (OASD-PA)
DEPARTMENT OF DEFENSE

00005012

"The views and conclusions contained in this document are those of the authors
and should not be interpreted as representing the official policies, either
expressed or implied, of the Defense Advanced Research Projects Agency or the
U.S. Government."

86 1 08 066

85 11 27 001

12

A Final Technical Report

from

CHARLES EVANS & ASSOCIATES
1670 South Amphlett Blvd., Suite #120
San Mateo, CA 94402
(415) 572-1601

Development and Application of SIMS Characterization Techniques for the Study
of Impurities and Impurity Motion in (HgCd)Te and CdTe

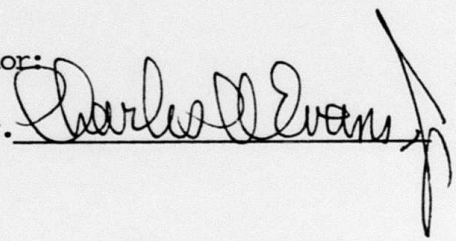
sponsored by:

Defense Advanced Research Projects Agency (DOD)
ARPA Order #4606

Under Contract #MDA903-82-C-0427 by Department of the Army,
Defense Supply Service-Washington,
Washington, DC 20310

Principal Investigator:

Charles A. Evans, Jr.
President



Effective Date: November 1, 1983

Expiration Date: September 30, 1985

Reporting Period: November 1, 1983 - September 30, 1985

"The views and conclusions contained in this document are those of the authors and should not be interpreted as representing the official policies, either expressed or implied, of the Defense Advanced Research Projects Agency or the U.S. Government."

86 1 08 066

86 35 1/108 066 01

EXECUTIVE SUMMARY

Accession For	
NTIS CRA&I	<input checked="" type="checkbox"/>
DTIC TAB	<input type="checkbox"/>
Unannounced	<input type="checkbox"/>
Justification <i>will be filed</i>	
By _____	
Distribution /	
Availability Codes	
Dist	Avail and/or Special
A-1	



EXECUTIVE SUMMARY

↓
The tasks in the Statement of Work for ^{this} Contract MDA 903-82-C-0427 were:

1. Develop quantitative methods of secondary ion mass spectrometry (SIMS) analysis; and
2. Study the incorporation and redistribution of impurities in (HgCd)Te and CdTe.

↓
The second task included investigation of MeV ion implantation into (HgCd)Te and development of image processing techniques for potentially quantitative investigation of laterally distributed impurities. These tasks were added after letting the original contract.

These tasks were fulfilled by:

1. Thorough investigation of peculiarities of SIMS analysis of (HgCd)Te, culminating in a protocol for specific analyses of Hg, transition element impurities and charging substrates;
2. A list of ion yield calibration factors (relative sensitivity factors) for twenty one (21) elements in (HgCd)Te and CdTe;
3. A finding that MeV ion implantation in (HgCd)Te is feasible, though not without caveats; and
- 4) Use of image processing as developed for use with the technique of SIMS imaging as a valuable, almost essential aspect of the study of (HgCd)Te.

↓
The mechanisms and protocols developed were applied to various kinds of (HgCd)Te and its homologs in the characterization of a variety of dopants and impurities of interest to DARPA and its subcontractors. These applications elucidated the mechanism of boron incorporation during the LEC growth of CdTe.

TABLE OF CONTENTS

Executive Summary.....	i
Introduction.....	1
Progress Summary.....	3
SIMS Analytical Procedures.....	4
Materials Research.....	8
References.....	13
Appendices.....	15
A Schematic of Camera IMS-3f.....	16
B Table of Relative Sensitivity Factors for SIMS Analysis of (HgCd)Te.....	17
C Least-Squares fits to RSF's vs. Ionization Potential and Electron Affinity.....	18
D Table of Mass Spectral Interferences for SIMS Analysis of (HgCd)Te.....	19
E1 Hg ⁺ Initial Kinetic Energy Spectrum.....	20
E2 Cd ⁺ Initial Kinetic-Energy Spectrum.....	21
E3 Te ⁺ Initial Kinetic-Energy Spectrum.....	22
E4 Te vs. Hg Initial Kinetic Energy Distribution.....	23
F SIMS Depth Profile Showing Laser Charge Reduction.....	24
G IKE Spectra of ¹⁶ O and ¹²⁰ Te Showing Laser Charge Reduction.....	25
H The Recognition Concepts Trapix Image Processing System.....	26
I Development and Application of SIMS Characterization Techniques for the Study of Impurities and Impurity Motion in HgCdTe and CdTe.....	27
J Development and Application of SIMS Characterization Techniques for the Study of Impurities and Impurity Motion in (HgCd)Te and CdTe.....	36
K Development and Application of SIMS Characterization Techniques for the Study of Impurities and Impurity Motion in (HgCd)Te and CdTe.....	43

INTRODUCTION

INTRODUCTION

The broad objectives and tasks under the scope of this contract were several:

I. SIMS Analytical Procedures

Develop quantitative analytical procedures for the application of high performance secondary ion mass spectrometry (SIMS) to the analysis of (HgCd)Te and CdTe for trace element and major constituent characterization, particularly Hg. This task included establishing a SIMS quantitation system, based on the relative sensitivity factor (RSF) approach. It also included examining the basis for several problems peculiar to SIMS analysis of CdTe and (HgCd)Te, with particular emphasis on the investigation of the ionization behavior of mercury.

II. Material Research

Perform materials-directed research in order to better understand the incorporation and redistribution of impurity elements in (HgCd)Te and CdTe. This research led to the finding that investigation of lateral segregation of impurities was of major importance, necessitating two changes to the original statement of work to investigate:

- A. MeV ion implantation for the preparation of standards, and
- B. Development of quantitative image processing as a tool for use with SIMS during (HgCd)Te analysis.

PROGRESS SUMMARY

PROGRESS SUMMARY

I. SIMS Analytical Procedures

A. SIMS Standardization

1. Overview

As is well known, the secondary ionization efficiency (directly affecting detection limits and quantitation) for a given element or species measured by secondary ion mass spectrometry (SIMS) is dependent on the element or species and the matrix from which it was sputtered. A schematic of the SIMS instrument used for these investigations is shown in Appendix A.

Quantitative analysis by SIMS requires the development of relative sensitivity factors (RSF's) to convert secondary ion currents or intensities into atomic concentrations. Therefore, a major thrust of this contract was the preparation and analysis of SIMS quantitation standards. Standards for SIMS analysis of semiconductor materials take one of two forms. The matrix of interest may be bulk doped with the impurity of interest during crystal growth; or wafer slices of the matrix may be ion implanted with controlled amounts of the impurity. The latter option was chosen for the present work, because uniformly bulk-doped (HgCd)Te and CdTe was unobtainable.

2. SIMS standards

The standards were prepared as unannealed ion implants into bulk CdTe and thick liquid phase epitaxial (LPE) (HgCd)Te. They were subsequently analyzed by

PROGRESS SUMMARY

I. SIMS Analytical Procedures

A. SIMS Standardization

1. Overview

As is well known, the secondary ionization efficiency (directly affecting detection limits and quantitation) for a given element or species measured by secondary ion mass spectrometry (SIMS) is dependent on the element or species and the matrix from which it was sputtered. A schematic of the SIMS instrument used for these investigations is shown in Appendix A.

Quantitative analysis by SIMS requires the development of relative sensitivity factors (RSF's) to convert secondary ion currents or intensities into atomic concentrations. Therefore, a major thrust of this contract was the preparation and analysis of SIMS quantitation standards. Standards for SIMS analysis of semiconductor materials take one of two forms. The matrix of interest may be bulk doped with the impurity of interest during crystal growth; or wafer slices of the matrix may be ion implanted with controlled amounts of the impurity. The latter option was chosen for the present work, because uniformly bulk-doped (HgCd)Te and CdTe was unobtainable.

2. SIMS standards

The standards were prepared as unannealed ion implants into bulk CdTe and thick liquid phase epitaxial (LPE) (HgCd)Te. They were subsequently analyzed by SIMS to establish a relationship between the known amount of ion element implanted versus SIMS ion yield. The relationship between a given known impurity concentration and its secondary ion yield in a particular matrix, known as a relative sensitivity factor (RSF), is multiplied by subsequent secondary ion intensity measurements from unknown samples, to obtain atomic densities or concentrations.

3. Drawbacks with the RSF approach

Quantitation by standards preparation has an important drawback, i.e., the ability to quantitatively analyze elements not prepared as standards. Though over twenty one (21) elements were successfully implanted and analyzed in (HgCd)Te, there remains the general problem of extending quantitation to the

rest of the periodic table. An accepted approach to extension of quantitation to all elements is to plot the RSF's obtained from standards versus some other elemental property, as it affects the ionization process, such as ionization potential (I. P.) or electron affinity (E. A.) [1]. The original RSF's and the plots that resulted constitute respectively, Appendices B and C.

B. Analytical Protocol Development

1. Overview

A fundamental reason for proposing this research was the observation that the SIMS analysis of (HgCd)Te and CdTe was more difficult than other semiconductor materials examined by this technique [2,3]. These difficulties included irreproducible Hg^+ intensity measurements, unusual mass spectral interferences and significant substrate charging effects. Thus, other than the above RSF quantitation efforts, most of the work under this contract went to establishing SIMS analytical protocols for (HgCd)Te and CdTe.

Mercury has been observed to have unusual ion yield characteristics. These phenomena have been extensively discussed in our previous reports [4]. The observed SIMS ion yield for Hg appears to be dominated by some other process besides the normal ionization process accompanying sputtering. The main evidence for this is the observation that the bulk of the Hg ions are produced with less kinetic energy than that which would be imparted by the ion extraction field (4500 V). This implies the ions form in the space above the sample, thereby achieving less than the full kinetic energy. This is not a "conventional" SIMS ion formation process, where the ions are formed at the sample surface during the sputtering event. Further evidence was obtained by investigation of the Hg lateral energy spread (i.e., the kinetic energy manifested in the diameter of the ion bundle). The lateral kinetic energy distribution for Hg^+ was found to be unusually low, suggesting that the Hg is thermally sublimed and then ionized in the gas phase.

Mercury cadmium telluride is unusual for a semiconductor in that the constituent elements are high in mass, relative to silicon. The effect of the heavy substrate elements is to cause significant spectral interferences due to multiply-charged ions of the matrix elements. Specifically, multiply-charged Hg, Te and Cd mass peaks interfere with the analysis of the transition elements. The interferences are listed in Appendix D. The interferences of practical importance are in the analysis of Fe, Mn, Ni, Zn and Cu.

A persistent analytical problem is the tendency for electrical charging to occur during depth profiling of (HgCd)Te on semi-insulating CdTe. This

introduced drifts in the measured ion intensities or currents during a profile not resulting from actual compositional changes.

As a consequence of these findings, a number of analytical method and tools have been developed. These are briefly reviewed here.

2. Protocol for the analysis of Hg in (HgCd)Te

A comparison of plots showing ion intensity versus ion initial kinetic energy for Hg^+ , Cd^+ , Te^+ and Si^+ reveals an important difference in the Hg^+ spectrum. This comparison is shown in Appendix E. Initial kinetic energy plots of this type indicate where the ions form. That most of the ions form at the sample surface is shown by the peak in intensity at 4500 V, which is the acceleration and extraction field in the spectrometer. That is, the ions are accelerated through the full field. The Hg^+ plot shows that the maximum amount of Hg^+ ion production does not occur at the sample surface, as is common with most ion production by SIMS. Rather, the bulk of the Hg^+ ions are produced in a region of space above the bombarded surface, as though leaving the sample as neutral particles. Further investigation of this phenomena revealed that ionization occurs to an important degree for Hg through "gas phase" interaction with the primary sputtering beam (O_2^+).

The explanation for the irreproducible Hg^+ ion yields was then clear. The bulk of the Hg ion signal arrived right at the edge of the spectrometer energy acceptance window. Small charging effects (discussed in more detail below) caused the signal to shift in and out of the window, resulting in large variations in the measured signal strength. The protocol developed to overcome this problem was to measure the Hg^+ ion kinetic energy spectrum for each sample prior to depth profile analysis. With this spectrum in hand, it was a simple matter to then select an appropriate bias voltage (energy offset) that would shift the bulk of the Hg^+ ions solidly into the energy acceptance window so as to not be affected by minor amounts of charging.

3. Protocol for transition elements analysis in (HgCd)Te

The problem of resolving the multiply charged ions of Cd, Te and Hg from the singly-charged ions of interest is one of a subset of spectral interference problems that plagues SIMS. Several standard techniques exist to resolve trace impurities peaks from the spectral interferences caused by substrate species ions. One of these employs the technique of energy filtering. This technique is usually used to discriminate against polyatomic or "molecular" ions containing one or more atoms from the matrix element(s). This method works because the molecular ions have a narrow energy distribution, compared to atomic ions. This means molecular ions can be effectively discriminated

against on the basis of their energy, at a small expense in loss of the atomic ion. The technique is usually used only to discriminate against molecular ions because most multiply-charged ions have energy distributions that are more broad than atomic ions.

In the case of (HgCd)Te, some of the unusual aspects of the ion yield can be used to advantage with the energy discrimination technique. During investigation of the relationship of ion yield versus kinetic energy for the singly- and multiply-charged ions of Cd, Te and Hg it was discovered that the multiply-charged ions of Cd and Te have the same distribution as singly-charged Hg^+ (see Appendix E). This fact allows the use of the energy discrimination technique which is normally ineffective against multiply-charged ions. The same approach used to shift Hg^+ ions into the energy acceptance window was now used to shift the interferences out of the window, by applying a bias of opposite polarity to that used for Hg^+ signal enhancement.

4. Protocol for signal shifts due to charging

Mercury cadmium telluride is usually prepared as an epitaxial layer on semi-insulating CdTe. This means as one performs a depth profile through the (HgCd)Te to the CdTe, there is the potential for electrical charging of the sample as the profile reaches the substrate. Electrical Charging has the effect of artificially depressing ion yields as the ion distribution is shifted out of the energy band pass originally set when sputtering at the surface. Since charging can be a dynamic process, the instrument controller must periodically measure the ion signals as a function of kinetic energy and adjust the sample bias to maximize transmission of ions through the spectrometer energy window. At this point the full complexity and acute dependence on electrical state of the sample during the depth profile in (HgCd)Te becomes evident.

Complex control software was devised as a means to handle the simultaneous bias adjustments needed to:

- a. Maintain the energy deficient Hg^+ within the spectrometer energy band pass;
- b. Discriminate against the energy deficient multiply-charged ions when measuring the intensity of a transition element; and
- c. Maintain the energy reference at zero in the presence of charging.

This software allows the investigator to individually shift the energy distributions of various species at will during a depth profile, as well as

accomplish dynamic charge mitigation, making possible the simultaneous analysis of ionic impurities (Li, Na and K), transition elements (Cr, Fe and Ni) and matrix species (Cd, Te and Hg) for interface definition. This degree of control has rendered the depth profile analysis of (HgCd)Te a relatively routine matter, albeit requiring set up procedures not commonly used in a SIMS depth profile.

II. Materials Research

Besides developing protocols for the routine analysis of (HgCd)Te, a very important use of this contract was as a vehicle to pursue important related investigations. The results of these are summarized here.

A. MeV Ion Implantation

One difficulty encountered during the preparation and analysis of the ion-implanted standards mentioned above was contamination of the (HgCd)Te surface. Among its many unusual properties, (HgCd)Te is a very soft and fragile material. Good surface morphology and cleanliness, even when achievable, are very difficult to maintain throughout the process of handling and fabrication of devices. Worse yet is the state of as-grown LPE crystalline material. Examination of this type of material by Auger electron spectrometry (AES) and scanning electron microscopy (SEM) has revealed significant concentrations of various impurities mechanically trapped in surface imperfections and blemishes. However, as-grown LPE (HgCd)Te is relatively inexpensive and readily available, thus it was used for the quantitation effort previously discussed in Section I, above.

Surface contamination affects the accuracy of ion implant derived RSF's because ion implants into (HgCd)Te using conventional implanter energies do not penetrate far enough into the sample surface. That is, the implant range in (HgCd)Te is so shallow that ion counts due to surface impurities constitute a large fraction of the total signal measured. Appendix E indicates the problem.

Because of the difficulty of obtaining adequately implanted samples of (HgCd)Te for quantitation, the prospects for MeV ion implantation of (HgCd)Te were investigated. A modification to the original contract was allowed for this purpose. Since new effects appear at these implantation energies, the concepts were first tested using Si, a relatively well understood substrate. The results of this experiment were the subject of an extensive report which indicated that, while the technique was viable there remained questions to be

answered, even about Si, before the technique was unleashed on the complex (HgCd)Te substrate [5].

B. Post Sputter Ionization

One of the hypotheses to emerge from the investigation of the ion yield of Hg was that Hg was possibly present as an excited neutral atom in the space above the sputter front. What is more, further investigation of the energy spectra of a wide selection of elements indicated that most, if not all sputtered elements had some degree of "post-sputtering" ion formation. Importantly, the elements that showed the largest degree of "post-sputtering" ionization occurring were some of those having the poorest overall SIMS detection sensitivity, such as Sn and Hg. This led to the exciting possibility of increasing ionization (thus sensitivity) through some means, such as optically "pumping" them to ionization through use of an appropriate laser.

Accordingly, experiments were devised to test this idea. The prospect of increasing ion yield by ionization of excited neutrals opens up new possibilities for dramatically improving the detection limit for the problematic element. The initial method proposed was to bring laser illumination into the SIMS with a variety of geometries to enhance ionization. Thus, on a separate proposal a laser was acquired from the San Francisco Laser Center, (a non-profit organization supported by the National Science Foundation, NSF Grant No. CHE79-16250, and the National Institute of Health, NIH Grant No. P41 RR01613-02).

The available laser was a 6 W Ar ion laser which was used to test the concept, although calculations indicated that a laser operating in the UV portion of the spectrum would have been more appropriate. The laser proved very useful in testing the ability to introduce potentially ionizing illumination into the sample chamber of the SIMS with several geometries and intersection path lengths.

While no increase in ion formation was observed, a serendipitous finding did occur. The Ar ion laser proved to be quite effective in increasing ion yields from CdTe substrates. The speculation is that this happens because the laser populates the conduction band of the CdTe and makes electrons available for charge reduction. These effects are illustrated in Appendices F and G.

C. Quantitative Image Processing

During the period covered by this contract, it became obvious that some of the anomalies previously observed in depth profiles of various impurities by SIMS resulted from lateral segregation of impurities in a material assumed to be

laterally homogeneous. Thus, permission was obtained to pursue an additional task to develop quantitative SIMS secondary ion image analysis and related image processing. Imaging and image processing are powerful intuitive techniques for understanding what is happening during the analysis of a sample by depth profiling.

Secondary ion imaging is made possible by use of the properties of stigmatic double focusing in the secondary ion mass spectrometer. That is, the ion optics of the CAMECA IMS-3f are designed in such a way as to permit corrections for first order aberrations in ion energy and mass while maintaining a stigmatic ion image. Thus, ions which originate at a given point in the sputtered area preserve that spatial orientation through the spectrometer, allowing use of the spectrometer as an ion microscope.

Prior to the advent of this contract, use of SIMS imaging had often revealed very important facts, such as, that the distribution of a given impurity or dopant element was inhomogeneous at an interface. The interface between an epitaxial layer and the underlying substrate was found to be the site of particle incorporation. This information came, however, at the expense of loss of continuity in the depth profile used to locate the interface, as well as the inability to observe the dynamics of onset and disappearance of the laterally segregated impurity.

At this point it was obvious that an extension of the basic imaging concept was needed. Such an extension existed in the field of digital image processing. This technique was originally developed for enhancement of images returned from space probes. As such, a well established base of hardware and software existed to draw from, so that the technique could be implemented quickly in the laboratory. The hardware used was purchased concurrent to, but not as part of, this contract. The software development was financed under this contract and is further discussed in Appendix H.

We have employed SIMS in combination with digital image processing to study a variety of sample types of interest to DARPA. Some of these data were organized into a video tape for presentation at the DARPA (HgCd)Te and GaAs contractor's meetings in the spring of 1985. These include:

1. A sample of epitaxial CdMnTe on GaAs was obtained from Professor Jan Schetzina of North Carolina State University. This sample showed an anomalously high Na content at the surface and at the episubstrate interface. The indicated amounts of Na exceeded the amounts to be expected in MBE growth. Such distributions are common in SIMS analyses and are generally thought to arise from surface and interfacial contamination. In order to better illustrate these contamination peaks,

we performed image depth profiles by recording the secondary ion images of Na^+ as a function of sputtering time in order to elucidate the nature of the contamination.

The Na^+ images at the surface revealed that the sodium is highly segregated in a pattern characteristic of environmental particles (i.e., dust and/or dirt). As the sputtering process removed the outer layers of the epilayer, the microscopic particles are sputtered away and the Na pattern becomes uniform, characteristic of a homogeneous contaminant. As the sputtering front approached the episubstrate interface, a localized band of finely dispersed Na^+ intensity was found. This type of segregated impurity is thought to result from finely divided atomistic contamination, probably from incomplete cleaning.

In summary, the image processing was found to be quite useful in elucidating anomalous intensity/concentration peaks in a depth profile. The ability to view the lateral as well as the depth distribution of an impurity provides insight into the nature of the contamination as well as its source.

2. The second study employing SIMS digital image processing was of the boron content of Bridgman and LEC CdTe grown at Westinghouse under their DARPA contract. During conventional SIMS depth profiling, significantly higher levels of boron were observed in the LEC material as compared to the Bridgman CdTe. In addition, the boron intensity exhibited large excursions in intensity, in certain cases several decades over a few seconds or minutes of sputtering.
 - a. The Bridgman material showed less than a few counts of B^+ which corresponded to of the order of 10^{15} at-cm⁻³.
 - b. The first LEC CdTe showed relatively low B^+ intensity (10^{16} at-cm⁻³) but with rapid factor of 10 intensity spikes.
 - c. The second LEC CdTe sample showed a continuously high B^+ intensity with an occasional increase and decrease.
 - d. The third sample of LEC CdTe showed long term variations from 10^{16} to 10^{19} at-cm⁻³.

These samples were then examined with the image processor to determine if lateral segregation could be responsible for these bizarre data, i.e., large variations in ion intensity from an ostensibly homogeneous material. As illustrated in the video tape, lateral segregation of the boron was indeed responsible for the widely varying B^+ ion intensity.

The very low boron content of the Bridgman material was found to be homogeneous, probably in solid-solid solution. Sample two (the first LEC CdTe) was found to contain small, widely separated, boron-rich regions. The concentrations were elevated in boron by some two decades but not sufficiently to be an actual second phase or precipitate. This was confirmed by no decrease in the Cd^+ or Te^+ intensities. Sample C contained numerous boron-rich regions, continuously changing in location, so prevalent that the time average of the boron intensity was nominally constant with time. The fourth sample was most interesting in that it contained some of the above mentioned boron-rich regions. Most importantly, this sample contained sub-grain boundaries which were decorated with boron.

Upon reflection, the incorporation is attributable to the low temperature needed for the growth of CdTe and the increased viscosity of the B_2O_3 encapsulant. The boule and melt rotation in combination with the higher boric oxide viscosity causes small amounts of the boric oxide to be incorporated into the melt and hence into the growing crystal. Such an effect is not seen in the LEC growth of GaAs due to the higher growth temperature and consequently lower viscosity of the boric oxide. With this understanding of the mechanism of boron incorporation, the viscosity of the boric oxide at the CdTe growth temperature was reduced with additives to reduce the boron incorporation.

3. The third image processing application was the study of segregation in doped GaAs. Howard Lessoff of NRL has shown unusual defects upon highlighting with a special etchant. In an indium-doped GaAs sample from Westinghouse, this feature was found to contain a slightly elevated concentration of indium (40% above the otherwise uniform doping level). Other doped sample (Cr and Si) containing these defects demonstrated no segregation as did the indium. However, the Cr and Si concentrations were significantly below that of the indium. No explanation for this phenomenon has yet been developed.

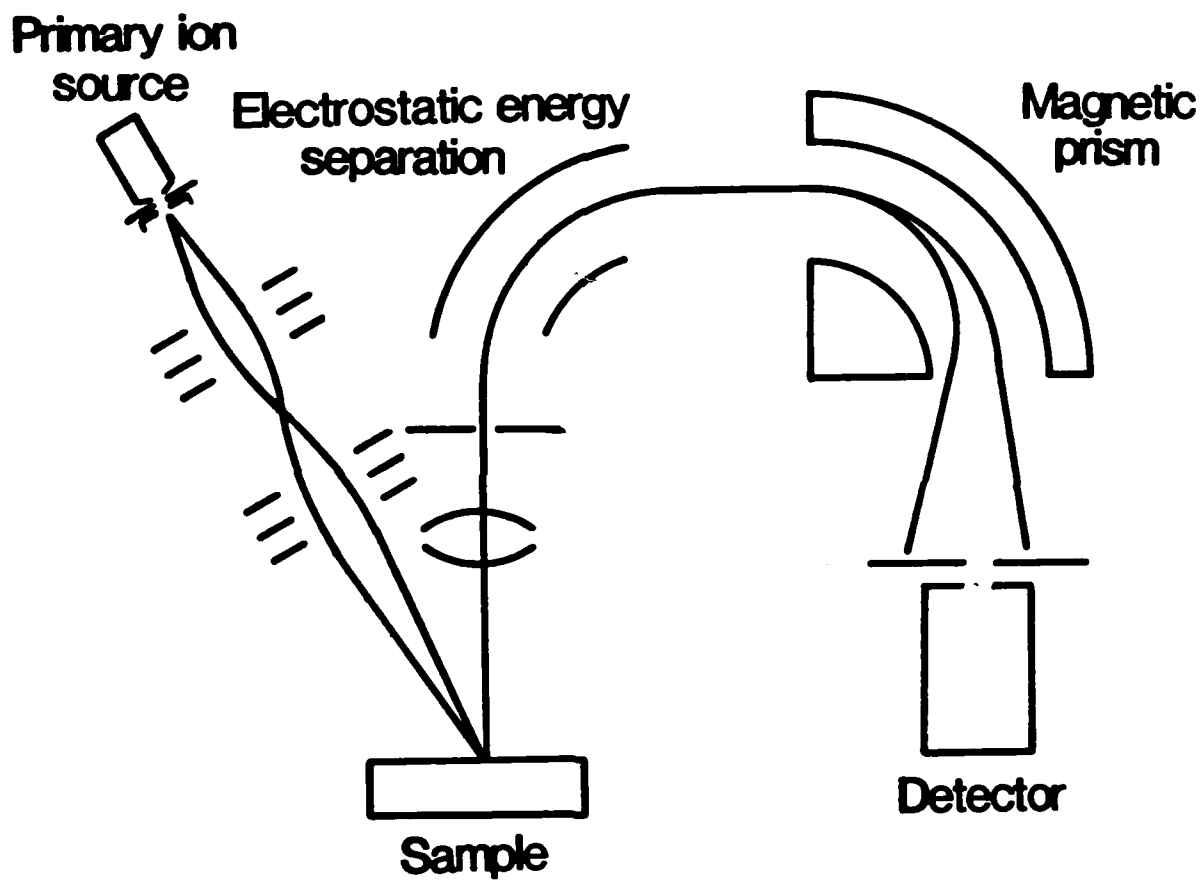
REFERENCES

REFERENCES

1. C. A. Anderson, J. R. Hinthorne, "Thermodynamic Approach to the Quantitative Interpretation of Sputtered Ion Mass Spectra," 45 (8), 1421-1438 (1973).
2. E. Holland, G. Blackmore, "Application of SIMS to Heavy Metal Tellurides," Surface and Interface Analysis, V4 N4, 174-177 (1982).
3. E. Holland, G. Blackmore, "Quantitative Application of SIMS to Cadmium Mercury Telluride," Int'l Journal of Mass Spectrometry and Ion Physics 46, 527-530 (1983).
4. Development and Application of SIMS Characterization Techniques for the Study of Impurities and Impurity Motion in (HgCd)Te and CdTe," Report #2 (11-1-82 to 5-1-83), Report #6 (11-1-83 to 5-1-84). The reports are attached, for convenience as Appendices I and J.
5. Development and Application of SIMS Characterization Techniques for the Study of Impurities and Impurity Motion in (HgCd)Te and CdTe," Report #8 (5-1-84 to 11-1-84). This report is attached, for convenience as Appendix K.

APPENDICES

SCHEMATIC OF IMS-3f

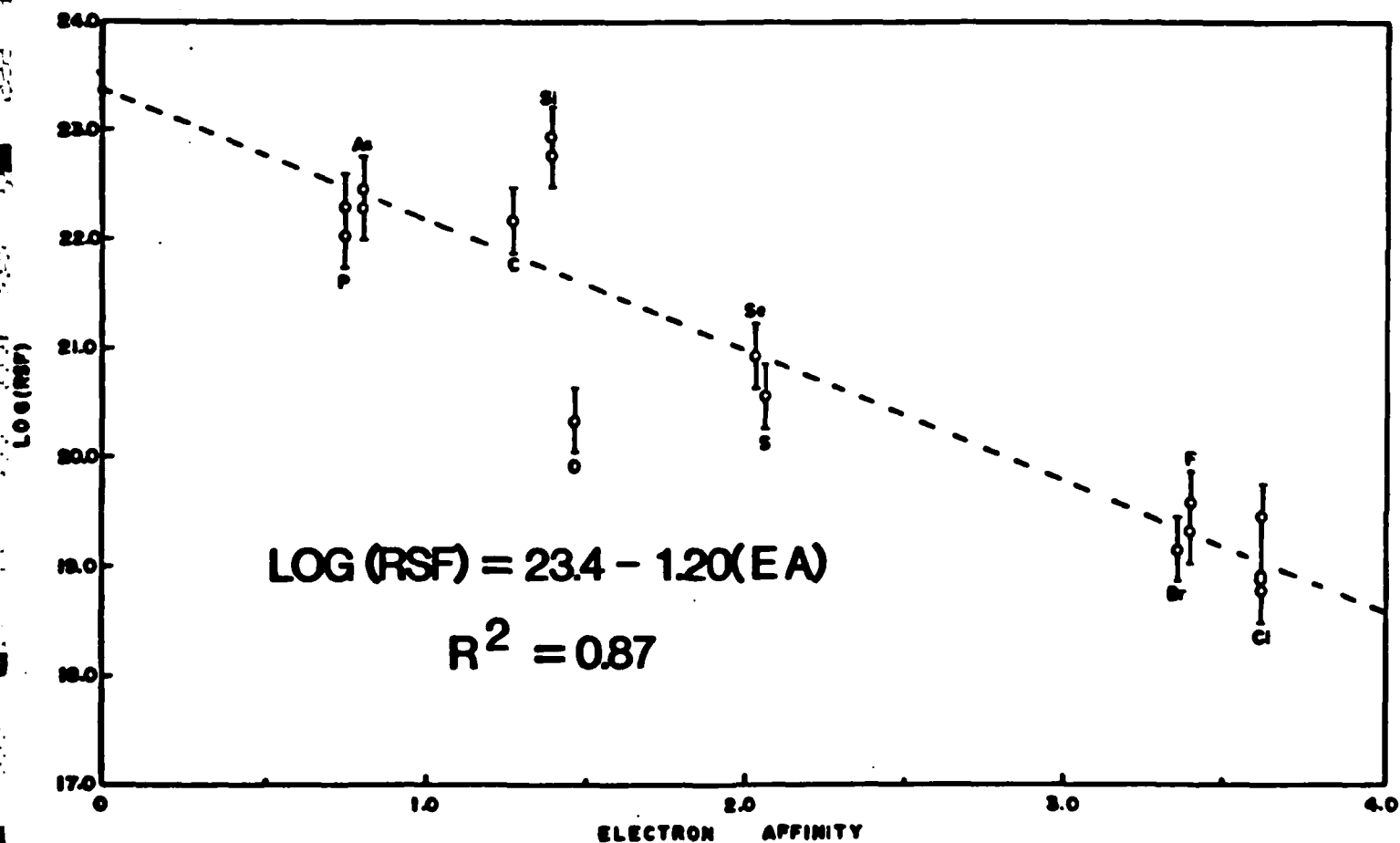
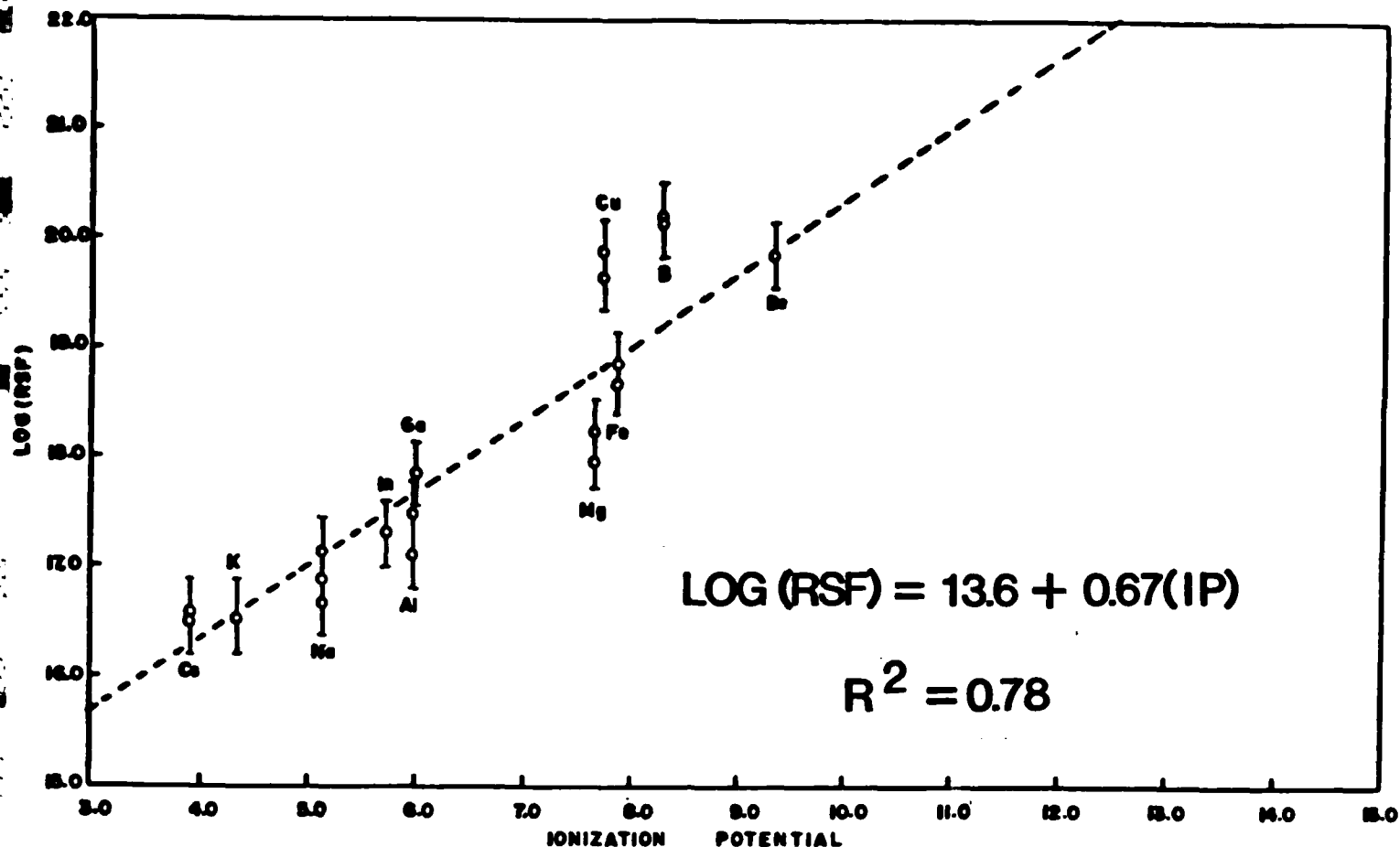


APPENDIX B

TABLE 1. Relative Sensitivity Factors For Selected Elements In (HgCd)Te

Element	Analysis Number			
	1	2	3	4
Be ⁺	7x10 ¹⁹			
B ⁺		1x10 ²⁰	2x10 ²⁰	
C ⁻	1x10 ²²			
O ⁻	2x10 ²⁰			
F ⁻	4x10 ¹⁹	2x10 ¹⁹		
Na ⁺	5x10 ¹⁶	1x10 ¹⁷	7x10 ¹⁶	
Mg ⁺	2x10 ¹⁸	1x10 ¹⁸	7x10 ¹⁷	9x10 ¹⁷
Al ⁺	3x10 ¹⁷	1x10 ¹⁷		
Si ⁻	8x10 ²²	6x10 ²²		
P ⁻	1x10 ²²	2x10 ²²		
S ⁻	4x10 ²⁰			
Cl ⁻	3x10 ¹⁹	8x10 ¹⁸	6x10 ¹⁸	8x10 ¹⁸
K ⁺	3x10 ¹⁶	4x10 ¹⁶	3x10 ¹⁶	
Fe ⁺	5x10 ¹⁸	5x10 ¹⁸		
Cu ⁺	4x10 ¹⁹	8x10 ¹⁹		
Ga ⁺	7x10 ¹⁷	8x10 ¹⁷		
As ⁻	3x10 ²²	2x10 ²²		
Br ⁻	1x10 ¹⁹			
Se ⁻	8x10 ²⁰			
In ⁺	2x10 ¹⁷	3x10 ¹⁷	1x10 ¹⁷	
Cs ⁺	3x10 ¹⁶	4x10 ¹⁶		

APPENDIX C



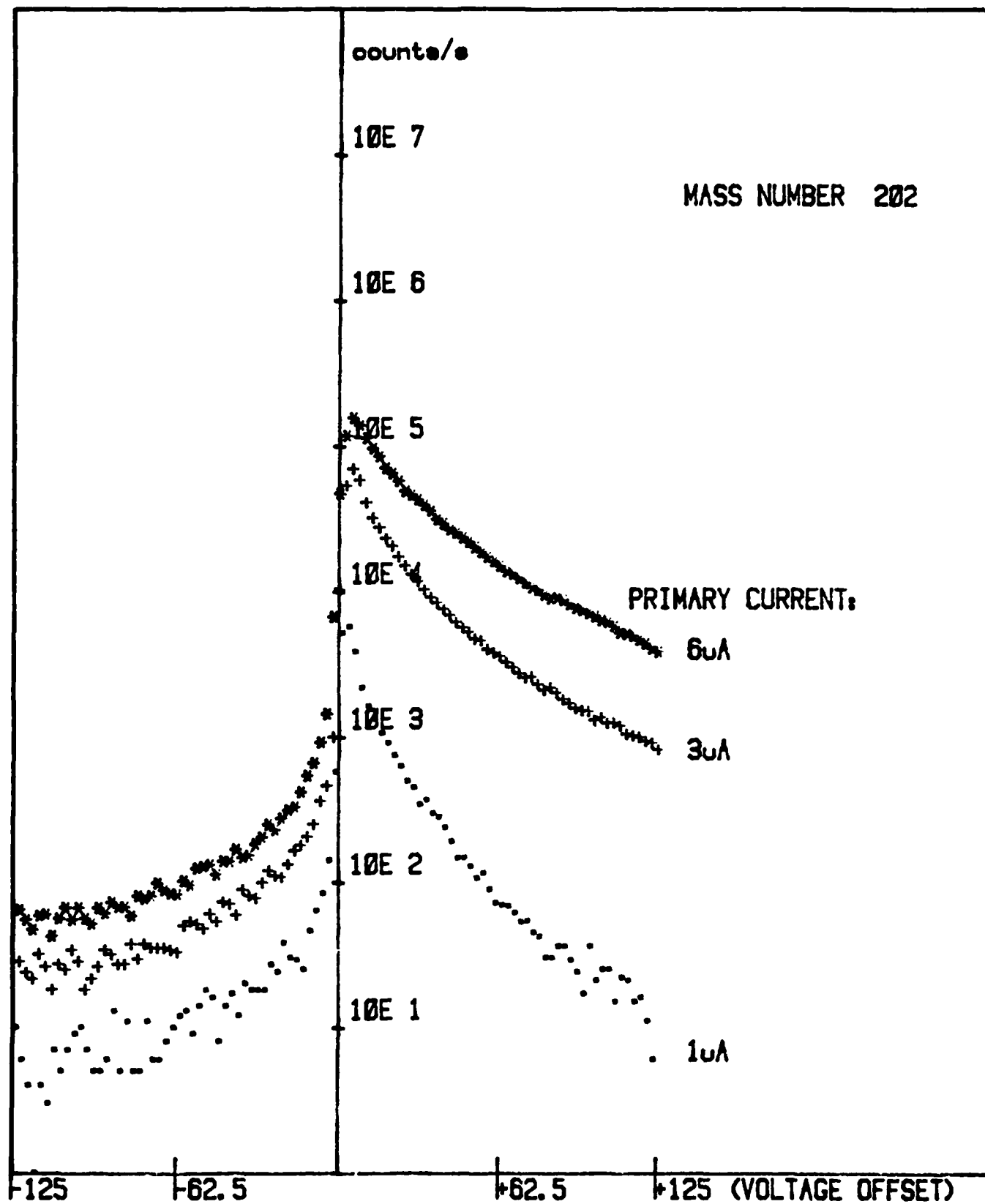
LEAST SQUARES FITS TO MEASURED RSF'S

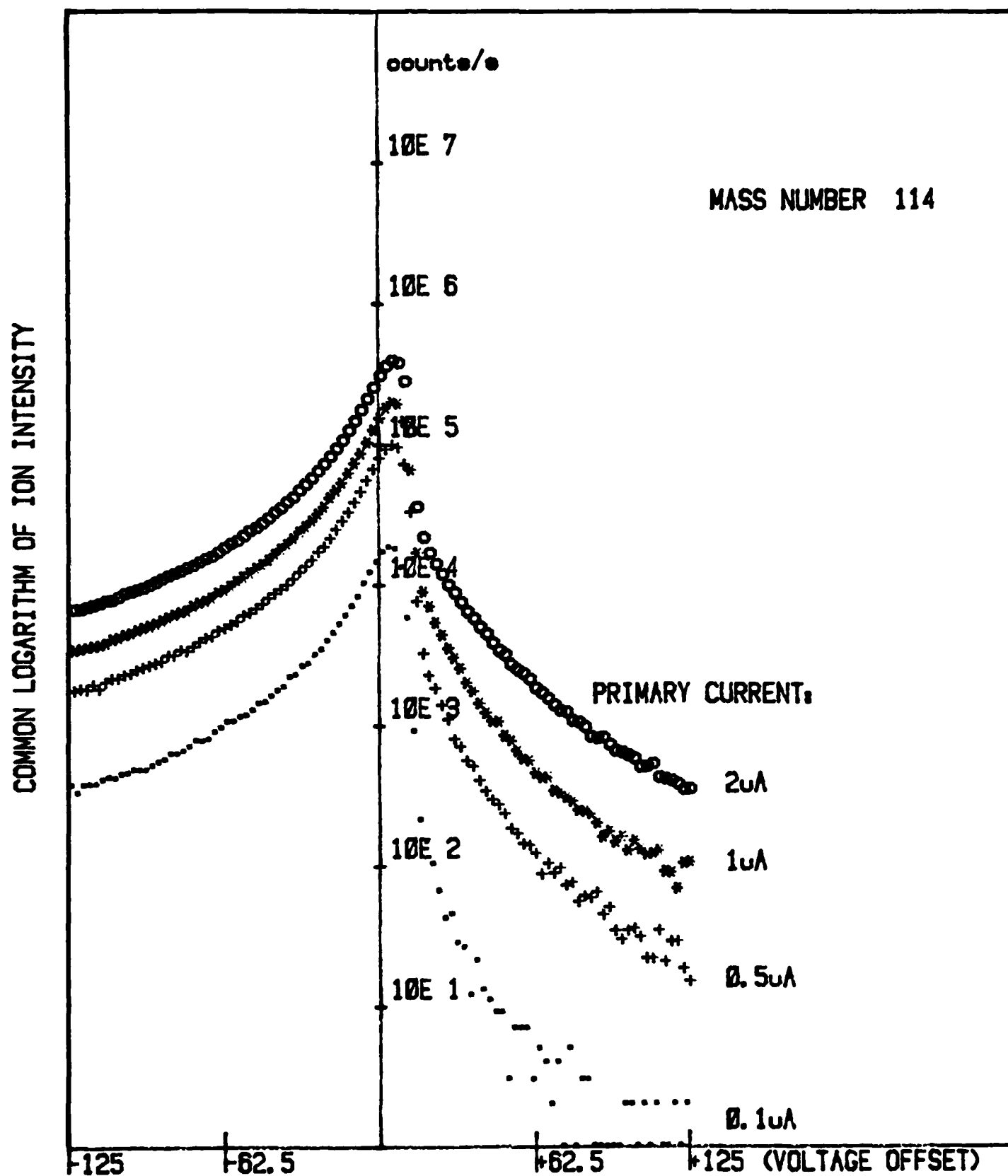
APPENDIX D

TABLE 2. Transition Element Interferences in (HgCd)Te Analyzed by SIMS.

<u>I</u>	<u>Abundance</u> (%)	<u>I/2</u>	<u>Species Interfered</u> <u>With</u>	<u>I/3</u>	<u>Species Interfered</u> <u>With</u>
(Cd) 106	1.22	53	⁵³ Cr		
108	0.88	54	⁵⁴ Cr, ⁵⁴ Fe	36	³⁶ S, ³⁶ A
110	12.4	55	⁵⁵ Mn		
111	12.8			37	³⁷ Cl
112	24.1	56	⁵⁶ Fe		
113	12.3				
114	28.9	57	⁵⁷ Fe	38	³⁸ A
116	7.58	58	⁵⁸ Fe, ⁵⁸ Ni		
(Te) 120	0.089	60	⁶⁰ Ni	40	⁴⁰ A, ⁴⁰ K, ⁴⁰ Ca
122	2.46	61	⁶¹ Ni		
123	0.87			41	⁴¹ K
124	4.61	62	⁶² Ni		
125	6.99				
126	18.7	63	⁶³ Cu	42	⁴² Ca
128	31.8	64	⁶⁴ Ni, ⁶⁴ Zn		
130	34.5	65	⁶⁵ Cu		
(Hg) 196	0.146	98	⁹⁸ Mo, ⁹⁸ Ru		
198	10.0	99	⁹⁹ Ru	66	⁶⁶ Zn
199	16.8				
200	23.1	100	¹⁰⁰ Ru		
201	13.2			67	⁶⁷ Zn
202	29.8	101	¹⁰¹ Ru		
204	6.85	102	¹⁰² Ru	68	⁶⁸ Zn

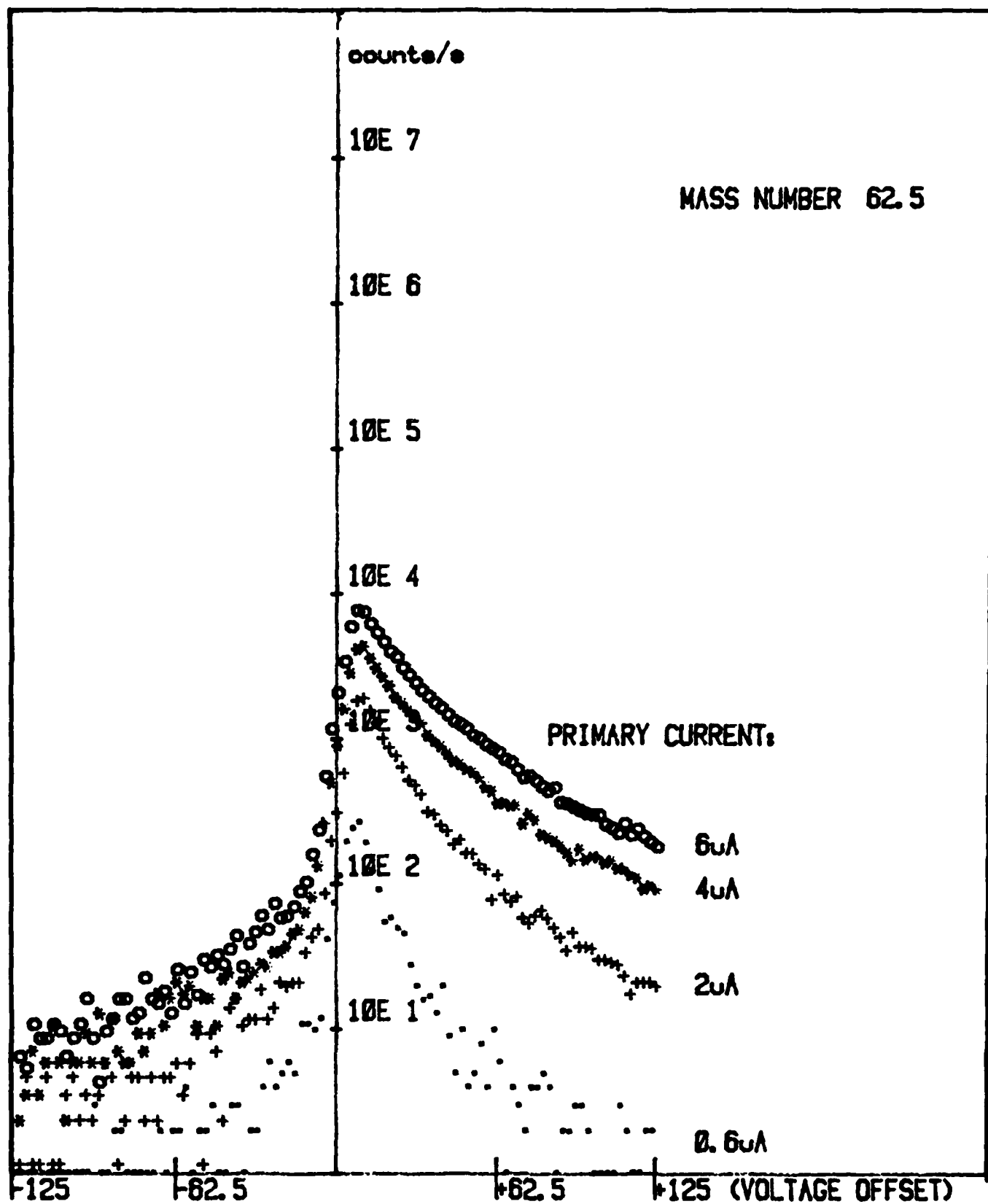
COMMON LOGARITHM OF ION INTENSITY

 $^{202}\text{Hg}^+$ ION INTENSITY VS. KINETIC ENERGY



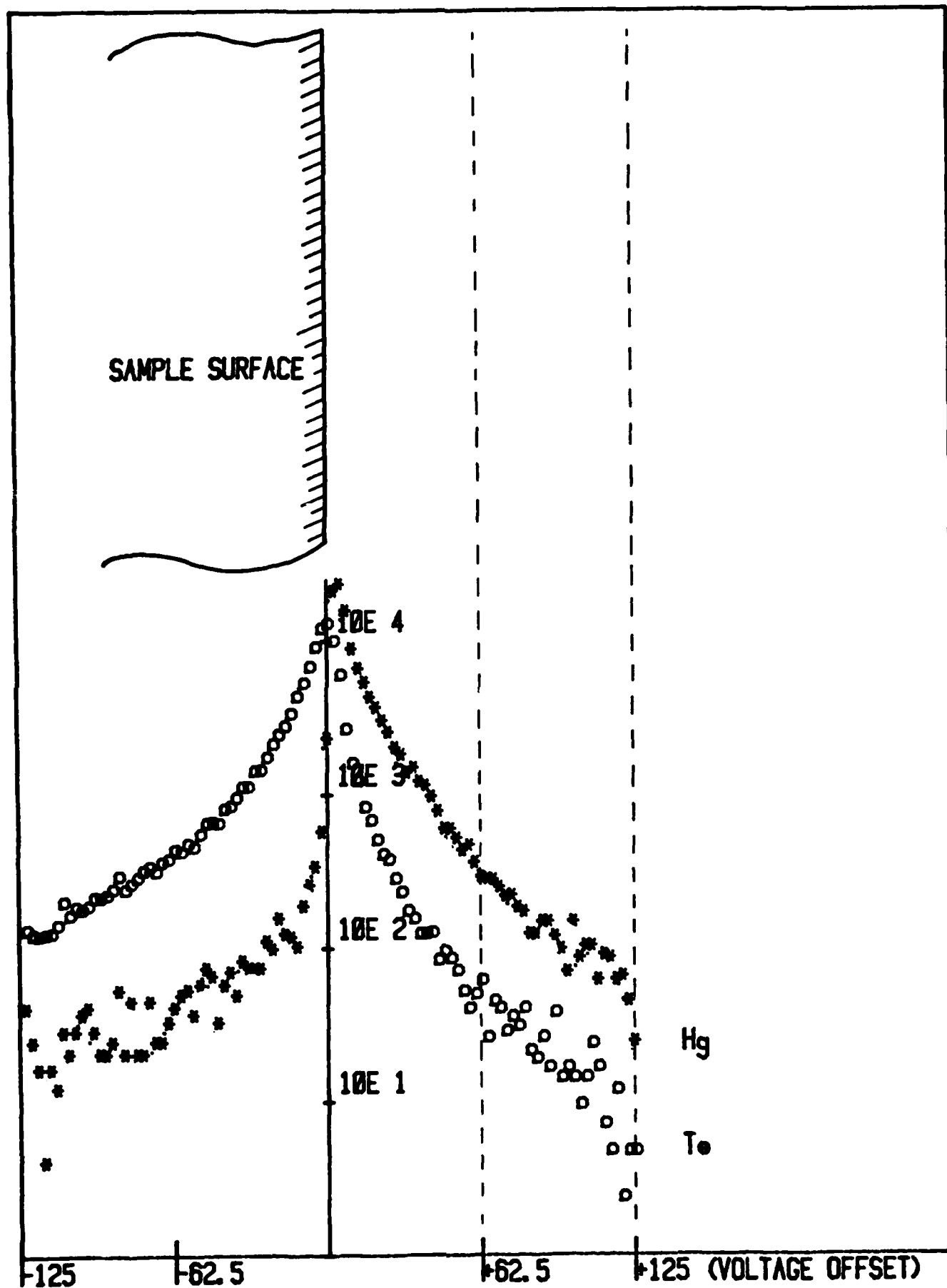
Cd ION INTENSITY VS. KINETIC ENERGY

APPENDIX E3



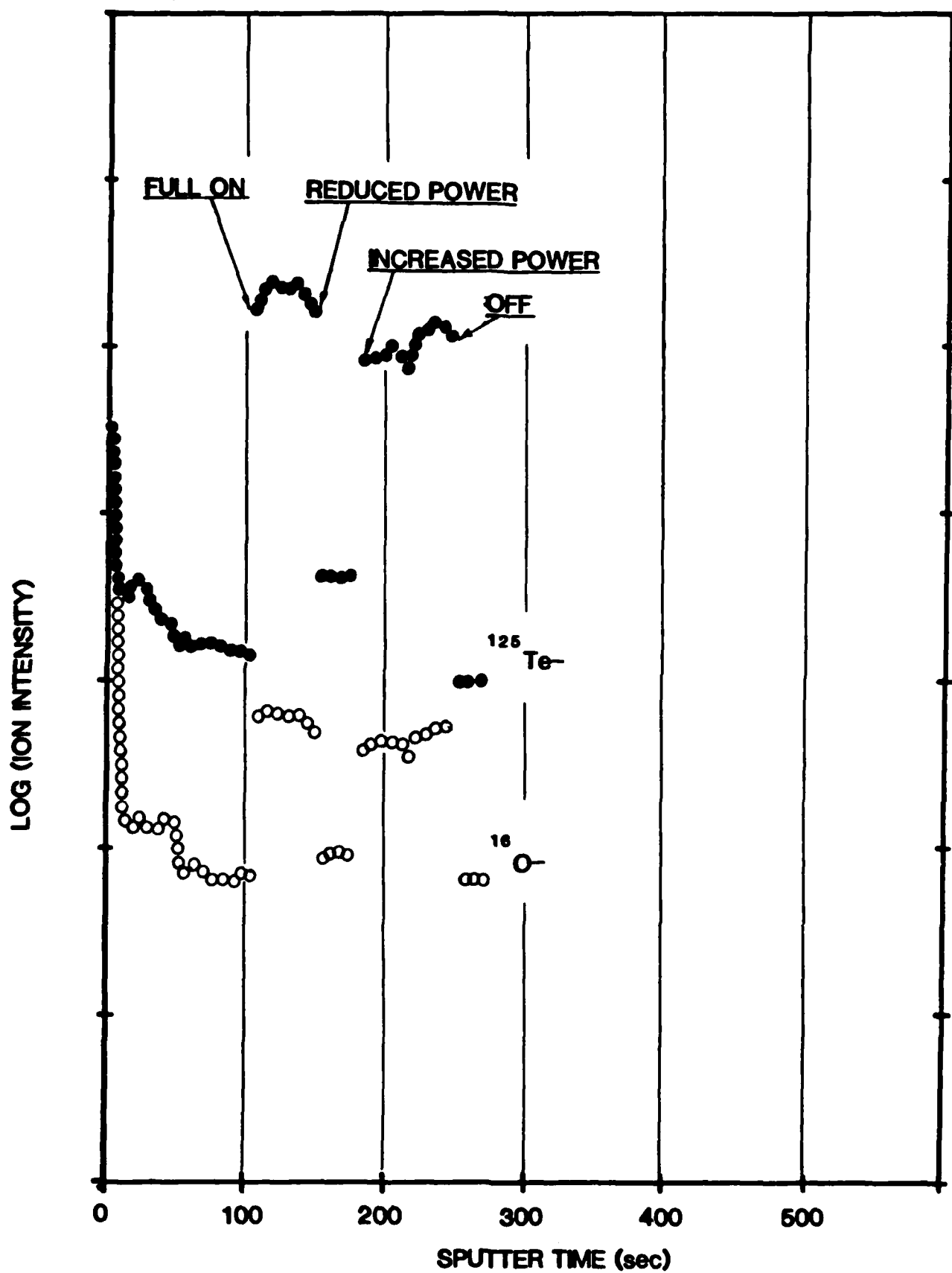
$^{130}\text{Te}^{2+}$ ION INTENSITY VS. KINETIC ENERGY

COMMON LOGARITHM OF ION INTENSITY



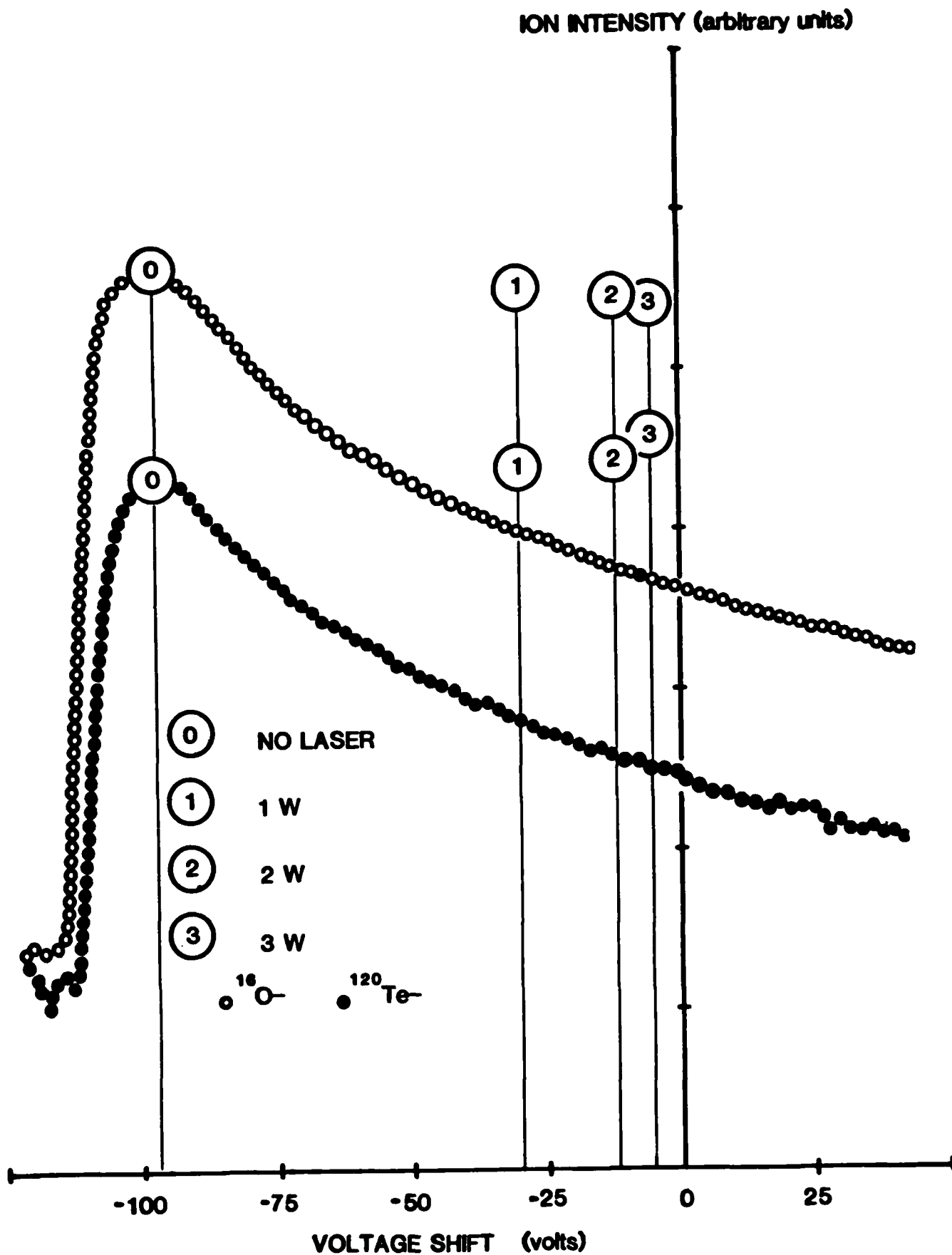
Te VS. Hg INITIAL KINETIC ENERGY DISTRIBUTION

APPENDIX F



SIMS DEPTH PROFILE SHOWING LASER CHARGE REDUCTION

APPENDIX C



IKE SPECTRA OF ^{16}O AND ^{120}Te SHOWING LASER CHARGE REDUCTION

APPENDIX H The Recognition Concepts Trapix Image Processing System

Image processing coupled with secondary ion microscopy has been developed and is routinely utilized for the determination of elemental composition of materials. A Cameca IMS-3f secondary ion mass spectrometer/ion microanalyzer, and a Recognition Concepts, Inc. (RCI) image processing system were both available to this contract at CHARLES EVANS & ASSOCIATES. However, image processing of ion microscopy data is an immature technology. Therefore, under the present contract, we have developed new software and operating methodology for the acquisition and manipulation of ion images. A major goal during this development was the quantitative measurement of the secondary ion intensities of images and preservation of that quantitative information for subsequent operations.

The available image processing hardware included the RCI Trapix 5500/64 image processor, a Digital Equipment Corporation LSI-11/73 host computer, and a Pulnix TM-34KA video camera. The image processor consists of the following:

1. Image memory. Two Mbyte of random access memory is organized so that it can be accessed at video speeds (7.9 MHz). Since each image consists of 512 x 512 pixel elements (pixels), and each pixel has eight bits of intensity information, it is possible to store eight images in the image processor memory. Image memory can be organized into 16-bit pixels when necessary.
2. A video digitizer. A 10-bit video digitizer converts camera intensity data to digital form at video rates.
3. A display driver and monitor. Three digital-to-analog converters provide outputs which control the three guns of a red-green-blue color monitor.
4. An arithmetic logic unit (ALU). The ALU manipulates image intensity data at the video processing rate. Possible functions include addition, subtraction, logical "and," "or," and "exclusive or," and the comparison functions (less than equal, not equal, etc.).
5. Several hardware look-up tables. These are memory banks which are inserted into the digital data stream and provide the capability of converting any pixel intensity (up to 12 bits) into any other pixel intensity which has been stored in the look-up table.

A host computer controls the flow of image processor functions and calculates the values to be stored in the look-up tables. The host computer consists of the following:

1. The LSI-11/73 central processing unit.
2. 512 kbyte of host computer random access memory.
3. A 140 Mbyte Winchester disk drive.
4. Dual 8" floppy disk drives.
5. Nine-track digital tape drive.
6. System terminal.

The Camesa ion microanalyzer is equipped with a dual microchannel plate/fluorescent screen image intensifier whose functions include converting ion current into electron current, amplifying the electron signal, and accelerating the electron beam onto an 18-mm fluorescent screen for visualization of the ion image.

The image processing system requires a video camera for detection of the fluorescent screen ion image. We evaluated several cameras and chose the Pulnix camera because it is the best combination of specifications including high light sensitivity, low frame-wide variation in background signal, low camera pattern background, and good flexibility of control. Two 35 mm camera lenses (with 85 mm and a 24 mm focal lengths), connected using their filter rings, provide the necessary magnification of the dual microchannel plate ion image.

A large amount of new software has been prepared for the image processor. The programs were designed to be easy to use and most functions require a single key stroke. The new routines can be divided into image acquisition routines, image manipulation procedures, and auxiliary control and utility features. The methods available for image acquisition include:

1. A "live frame" mode in which the monitor is continuously refreshed with current video data. This mode is used for setting up the ion microanalyzer.
2. A camera frame integration capability in which multiple frames of video data are accumulated by a 16-bit buffer. The 16-bit intensity data is usually scaled to the brightest pixel with calculation of a quantitative

scale factor. Alternatively, the 16-bit data can be scaled using a square-root function, a logarithmic function, or not scaled at all.

3. A "formatted" image acquisition mode in which an incoming camera image is reduced in size (formatted) and stored in a region of the image display. Different format sizes provide for the display of 4, 16 or 64 reduced images each in a "box" on the main display screen. Each new frame of camera data is reduced and stored in the next "box" at a timed interval until the entire frame is filled. Camera data integrated over several video frames can also be formatted.
4. A timed sequence mode of image acquisition which provides for automatic storage of images produced at regular intervals. This mode and the formatted mode are often utilized to provide a temporal record of image changes resulting from the sputtering process in the ion microanalyzer.

Camera frame integration has been implemented for the formatted and timed sequence modes. In all three acquisition modes, a post digitizer look-up table is available. The look-up table map in Figure 1 is commonly used to eliminate camera background noise. It is convenient to include the routines of image retrieval in the image acquisition menu. Single images as well as multiple images series can be recovered. A series of images can be recovered one by one with concomitant plotting of the total image intensity.

Once an image has been acquired or retrieved from disk storage, it can be manipulated and examined. Among the many useful procedures for working with single images is intensity scaling. In this procedure a band of grey levels is passed through a look-up table and converted to a different band of gray levels. For example, a narrow band of gray levels in a low contrast image can be converted into a wider band containing brighter and darker levels, thus enhancing contrast. A related procedure provides for image bit rotations, the equivalent of multiplication or divisions of image intensity by two. Another useful procedure is image convolution which provides a wide range of image enhancements, depending on input parameters. For example, the enhancements include pixel-to-pixel image noise reduction, and image edge enhancement. Examination of single pixels in an image can be accomplished using a cursor under interactive control, examination of pixel intensities along a line is provided by a line profile procedure, and the statistics and histogram of an image can be displayed by using the histogram function.

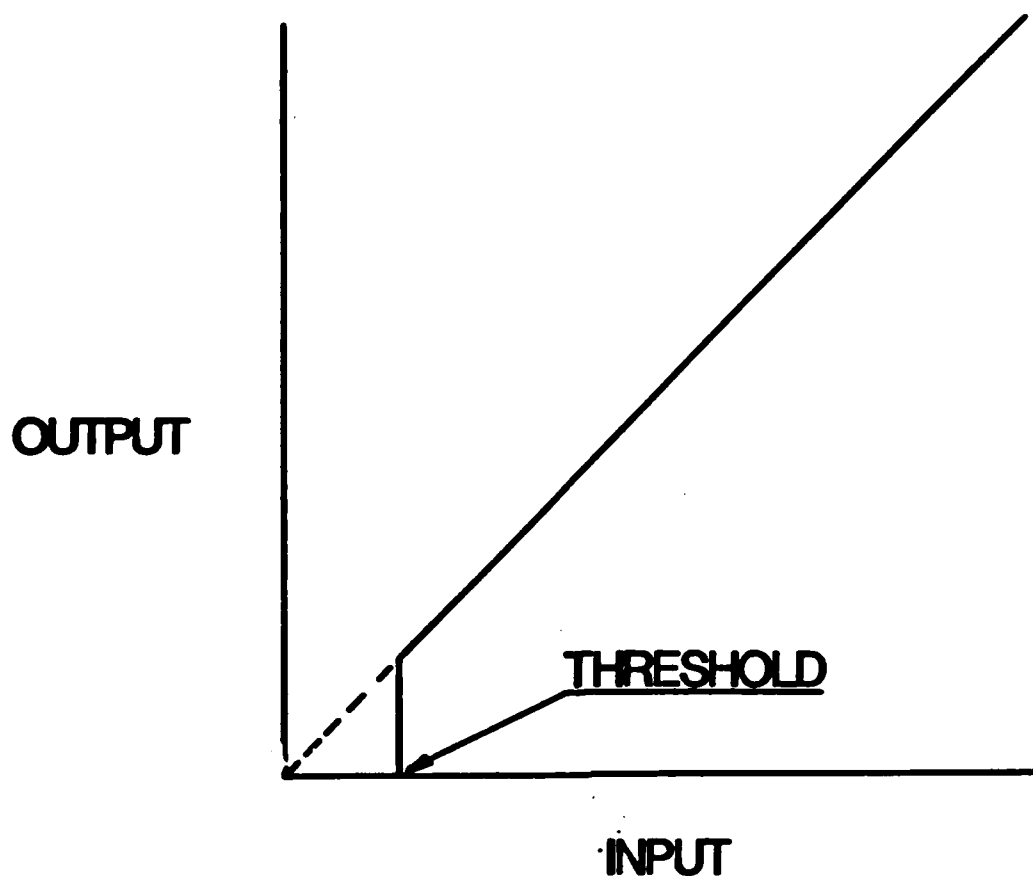


FIGURE 1. Linear Look-up Table Map With Noise Suppression Threshold.

A range of utility features provides auxiliary functions. The most commonly used functions are:

1. Image disk storage. The image and its associated parameters and character strings are included.
2. Image annotation. Labels of different sizes can be added to the image, moved around, edited, and changed in color.
3. Cursor, zoom, and scroll. These features are utilized during image examination.
4. Pseudocolor. Assignment of colors to the various gray levels makes visualization much easier.
5. Micrometer calibration bar. A crion scale can be added to ion microscope images.

OBJECTIVES

The broad objectives of this program are (1) to develop quantitative analytical procedures for the application of high performance secondary ion mass spectrometry (SIMS) to the analysis of CdTe and (HgCd)Te for trace element and major constituent characterization, particularly Hg, and (2) to perform materials-directed research in order to better understand the incorporation and redistribution of impurity elements in CdTe and (HgCd)Te.

PROGRESS SUMMARY

A. Analytical Procedures

1. Standardization

The major requirement for the quantitative analysis of impurity elements in CdTe and (HgCd)Te is the preparation of standards. Since SIMS is a relative technique, standards are prepared by ion implantation of the elements of interest into these matrices. The implants are being made under a subcontract to Dr. Robert Wilson of Hughes Research Laboratories, Malibu, CA.

In our initial attempts to depth-profile implants in CdTe, we encountered serious problems due to electrical charging under ion bombardment. Thus, these samples have been set aside until we can develop procedures to counteract charging effectively. (This topic is discussed in detail below.)

Other implants were prepared in (HgCd)Te. Since the implantable area of material available to us is small, Dr. Wilson implanted several ions into each sample. Depth profiles of the ions in these multiple-implanted samples had peculiar distributions, suggesting some difficulty with the (multiple) implantation into (HgCd)Te. No such effect was observed in depth profiles of similar species implanted together in Si, Ge or GaAs. Work is in progress to resolve this issue.

2. Mass and Energy Spectra

In the past six months, we have focussed on many preliminary aspects of analytical procedures development. Complete secondary ion mass spectra have been acquired from the II-VI compounds CdTe, (HgCd)Te, (ZnCd)Te and (MnCd)Te. These spectra were acquired using positive secondary ion spectroscopy (facilitated by O_2^+ primary ion bombardment) and negative secondary ion spectroscopy (performed by Cs^+ primary ion bombardment). Further, the effect of secondary ion initial kinetic energy discrimination was studied. Initial kinetic energy distributions were obtained for major constituents and for some doubly-ionized atomic ions and molecular ions.

The mass and energy spectra enabled the identification of the major spectral interferences in these matrices and the development of standard operating conditions to minimize the effect of spectral interferences. On the basis of these spectra, it became apparent that in Cd-bearing telluride compounds the matrix ion of choice for normalization should be $^{125}\text{Te}^{\pm}$ and not the ion of the major isotope $^{130}\text{Te}^{\pm}$ as had been previously used. Cadmium oxide molecular ions can "contaminate" the other major tellurium isotopes.

The most fruitful studies in this series were those on the initial kinetic energy distributions of the secondary ions emitted from the sputtered matrices. For most secondary ions, whether matrix level or impurity, the initial kinetic distributions begin at or near zero and extend over a range to higher initial kinetic energies. The width of this distribution is generally greater for singly and multiply-charged ions than for multi-atomic, molecular ions. We routinely take advantage of this phenomenon by using the voltage offset mode of SIMS, a technique which limits measurement to ions in a selected energy range. This process is used to reduce spectral interferences due to molecular ions with the same mass as the atomic ions of analytical interest. Generally, this technique is not as effective against interferences from multiply-charged ions, a dominant spectral problem in $(\text{HgCd})\text{Te}$ and CdTe , particularly multiply-charged Cd, Te and Hg at the masses of the transition elements.

Our results on the initial kinetic energy spectra of ions sputtered from these II-VI compounds provide essential, independent corroboration of important initial observations by Holland and Blackmore (1982).^{1,2} Unlike any other elements we had studied, the singly-charged Hg ion and multiply-charged ions of Cd, Te, Hg and Zn had kinetic energy distributions with little or no ions above zero eV initial kinetic energy. The energies of these ions begin at zero eV and are distributed over a range of energies extending significantly below zero. By recognizing that the multiply-charged matrix ions in CdTe and $(\text{HgCd})\text{Te}$ have "retrograde" energy distributions, we can use the voltage offset technique, not normally effective for multiply-charged ion interferences, to increase the signal to interference intensity ratio and thus greatly improve our detection limit for several of the transition element species.

In an effort to clarify the origin of such unusual secondary ion distributions, our measurements went beyond previous work to include Cs^+ and O^- ion bombardment, as well as O_2^+ ion bombardment. We observed that the ion yield versus energy of the singly-charged matrix species varies linearly with bombarding ion current density in the region of the energy spectrum from zero eV and up, regardless of bombarding species. (No results were obtained for Cd and Hg under Cs^+ bombardment since they do not form negative ions). The most significant observation was that in the region of the energy spectrum from zero eV and down, the ion yield of Hg^+ , Cd^+ and Te^{2+} vary quadratically with bombarding ion current density. The effect is shown as ion yield curves versus energy for Hg^+ , Cd^+ and Te^{2+} in Figures 1-3, respectively.

These studies indicate two causes for the irreproducibility of Hg^+ intensity measurements in previous studies.

As seen in Figure 1, the Hg^+ ions are mostly distributed at kinetic energies at or below zero eV, with a small number of ions appearing at zero and greater kinetic energies. Analysis of most species require the spectrometer to be set to accept ions of zero and greater kinetic energies. This fact, coupled with the commonly encountered electrical charging under ion bombardment which causes irreproducibility shifts in the entire energy spectrum of Hg, results in the poor reproducibility of mercury analyses. Secondly, Hg^+ ion production over most of its energy distribution depends quadratically on the bombarding ion current density, which unlike the ion current, is difficult to reproduce from day to day.

Thus, by purposely setting the instrumental parameters to efficiently collect the zero-and-below kinetic energy ions of Hg^+ , and by dynamically compensating for charging, we measure a more constant Hg^+ ion intensity. In combination with tight control on the instrument parameters governing bombarding current density, we expect to realize a return in much improved sample to sample reproducibility for Hg analysis.

3. Data Acquisition and Presentation

To some extent, implementing the above procedures to achieve improved analytical capabilities requires the application of novel data acquisition and presentation techniques in our analyses of these materials. These allow easier access to and better control over the considerable amount of information contained in a depth profile.

Control software has been developed to exploit the Cameca IMS-3f instrumental capability for determining the extent of sample charging during profiling of epitaxial layers. Charging can be compensated dynamically and a plot of voltage compensation versus depth prepared. This gives a valuable insight into the extent of charging during profiles of epitaxial layers on semi-insulating substrates, or any other structure. Thus, we can isolate artifacts which might relate to sample charging.

At the completion of each analysis, we can evaluate the total integrated counts for each impurity with matrix normalization. This is a quality-control feature which allows real-time comparison of experimental data with expected behavior or with other data.

Other routines can be used to prevent the very intense matrix ion signal from saturating the sensitive electron multiplier detector as the spectrometer magnet slews from impurity mass to impurity mass. This prevents a variable detector gain which manifests itself as instabilities in the ion intensities recorded for the species immediately beyond the intense matrix ion signal. Additionally, intensity versus depth data for selected matrix ions can be presented on linear scales, which helps to more closely monitor the variations in compound stoichiometry.

4. Materials Research

This phase of the research involves our collaboration with other research groups which specialize in materials growth and preparation. During this period we performed three materials related studies, with varying success, depending on the analytical behavior of each sample type.

We were provided a bilayer slider-grown LPE (HgCd)Te sample by the group under R.A. Wood at Honeywell, Minneapolis, MN. This sample was prepared so that there was a deliberate variation in x , the atomic fraction of Cd. We did not observe the growth variation when the sample was profiled using SIMS, but this work was done prior to the above-mentioned fundamental Hg studies. Therefore, armed with our new knowledge we will remeasure the sample and report the results at a future date.

Some cast CdTe was provided to us by Dr. R. Hilton of Amorphous Materials, Inc., Garland, TX for general examination and preparation suitable for ion implantation. This material provided most of the mass spectral data for molecular interferences and remains quite useful for a variety of purposes. Several pieces are being polished for ion implantation by the proprietary "hydroplaning" operation by Dr. T. Magee of Aracor, Sunnyvale, CA. We hope to report the progress on that aspect soon.

In collaboration with Prof. J. Schetzina of North Carolina State University, Raleigh, NC, we have applied SIMS to a variety of MBE grown CdTe layers on (HgCd)Te, InSb and sapphire substrates. The quality of this CdTe was very good and its semi-insulating properties made the analysis difficult. Some of the samples were sufficiently insulating to preclude analysis under positive ion bombardment. We are now planning repeating these analyses with gold coating and negative ion bombardment. The data from those that were analyzable is now being reduced and evaluated. These results will be reported in a future communication.

5. Significant Problems/Future Work

The greatest problem encountered during the initial analysis of these materials by SIMS was that of surface charging under ion bombardment. Except for epitaxial (HgCd)Te, all substrate and bulk CdTe, ZnCdTe, MnCdTe, etc., exhibited moderate to severe electrical charging. We anticipate that the next phase of our research will focus on this issue.

Several strategies, successfully employed in the past for analysis by SIMS of electrically insulating samples, are available. We anticipate studying the effects of:

- a. sputter-coating the samples with a conductive film

- b. simultaneous bombardment of the sample surface with an electron beam (during O_2^+ bombardment)
- c. using a Mo aperture placed over the areas of analytical interest
- d. use of O^- oxygen bombardment
- e. preparation of ion implants in electrically doped substrates as possible means to overcome the problem.

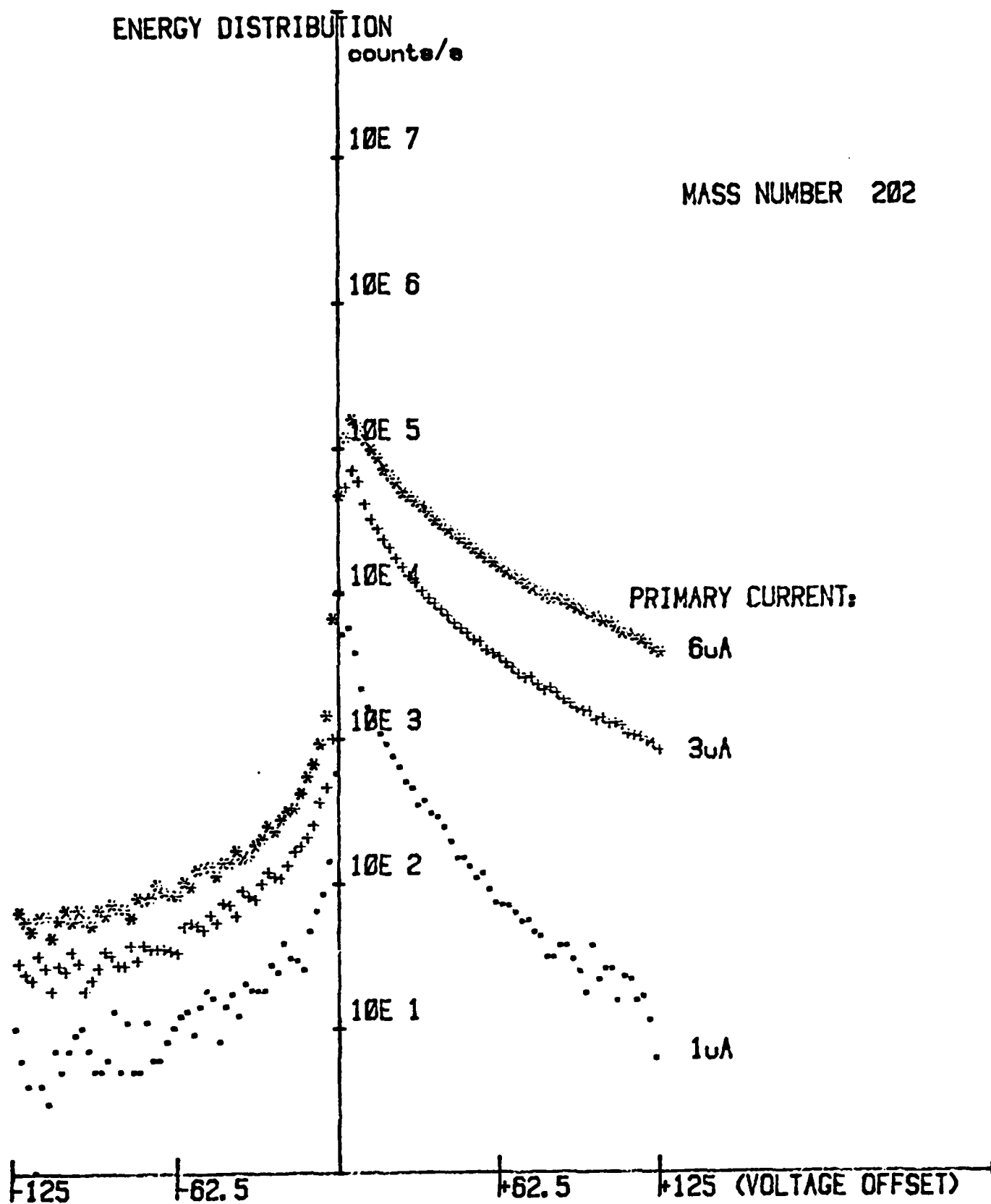


FIG. 1 Hg^+ ION INTENSITY VS INITIAL KINETIC ENERGY
FOR SEVERAL PRIMARY ION CURRENTS

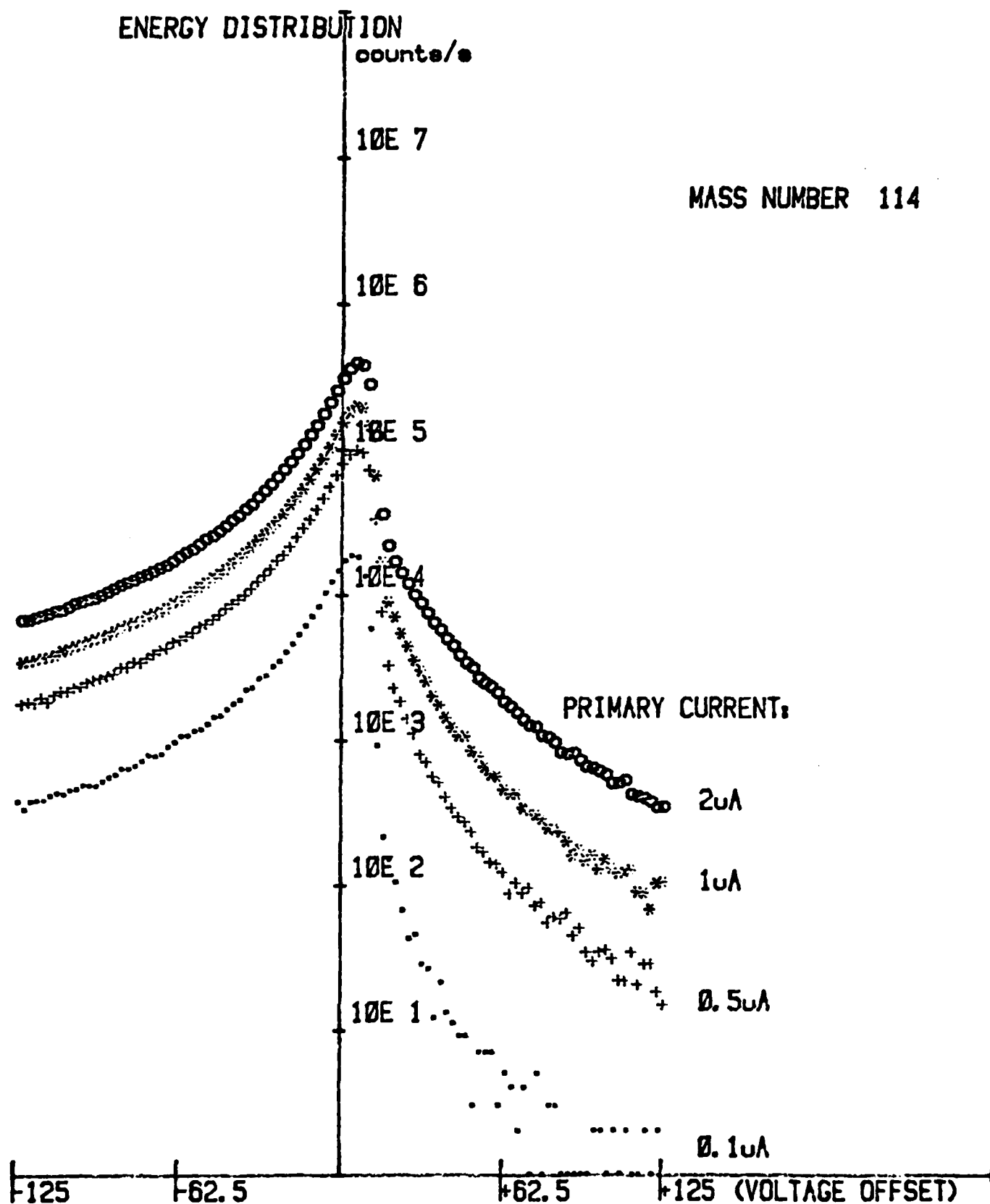


FIG. 2 Cd^+ ION INTENSITY VS INITIAL KINETIC ENERGY
FOR SEVERAL PRIMARY ION CURRENTS

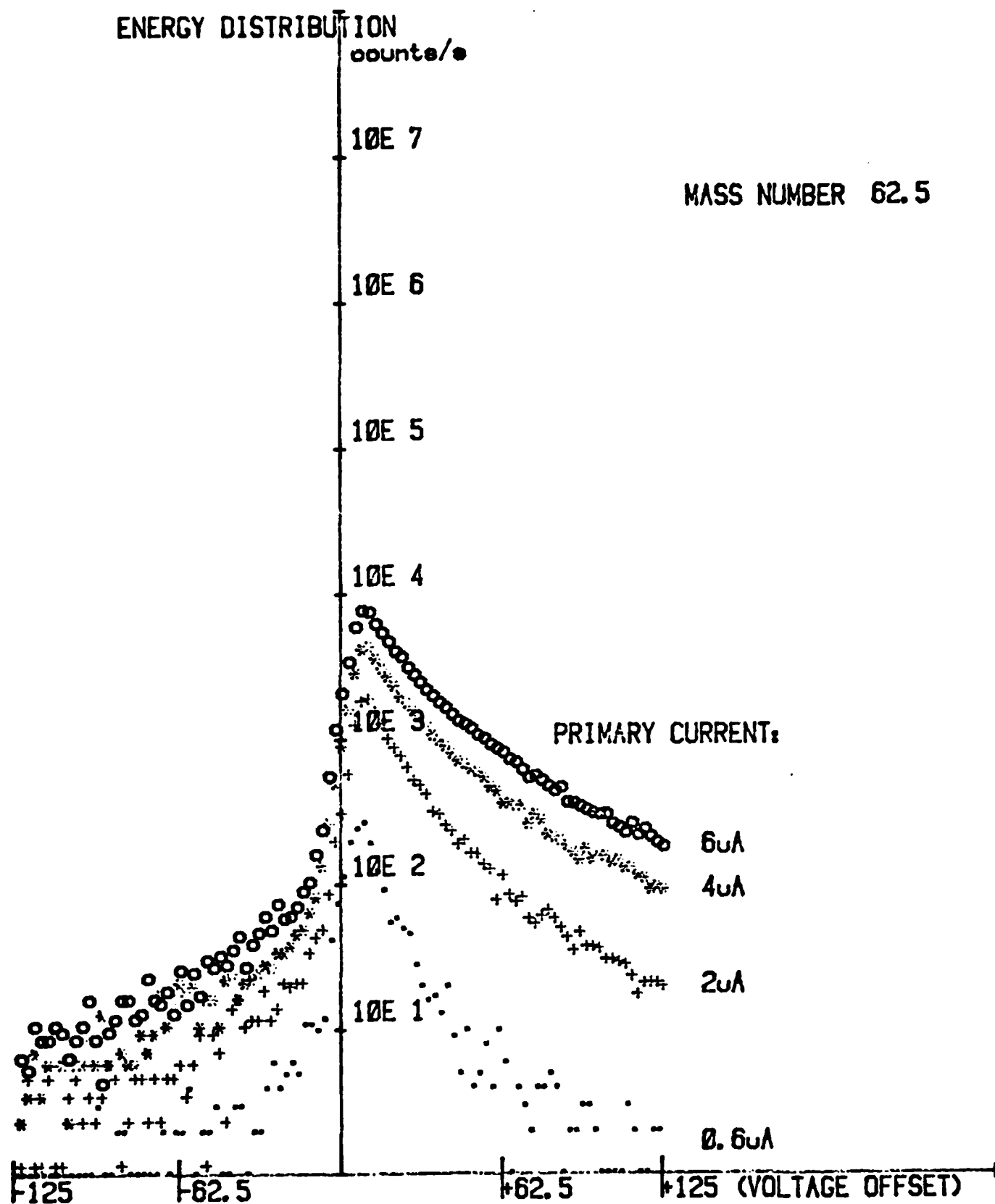


FIG 3. T_2^{2+} ION INTENSITY VS INITIAL KINETIC ENERGY
FOR SEVERAL PRIMARY ION CURRENTS

REFERENCES

1. Holland, E., Blackmore, G.W., "Application of SIMS to Heavy Metal Tellurides", Surface and Interface Analysis, Vol 4, Num 4, 174-177 (1982)
2. Holland, E., Blackmore, G.W., "Quantitative Application of SIMS to Cadmium Mercury Telluride", Int'l Journal of Mass Spectrometry and Ion Physics 46, 527-530 (1983)

OBJECTIVES

The broad objectives of this program are (1) to develop quantitative analytical procedures for the application of high performance secondary ion mass spectrometry (SIMS) to the analysis of CdTe and (HgCd)Te for trace element and major constituent characterization, particularly Hg, and (2) to perform materials-directed research in order to better understand the incorporation and redistribution of impurity elements in CdTe and (HgCd)Te.

PROGRESS SUMMARY

A. SIMS Analytical Procedures

Research into the application of SIMS to (HgCd)Te has been the main focus of work under this contract for the last 18 months. A major milestone of this project has been to develop quantitative methods for the characterization of (HgCd)Te by SIMS. That milestone has been reached with the release of the SIMS relative sensitivity factors in our previous two reports to DARPA and to the materials community at-large at the Third (HgCd)Te Workshop¹. This intensive effort has also clarified most of the difficulties with quantitative impurity analysis in (HgCd)Te by SIMS and rendered depth profiling this material a relatively routine procedure. During this reporting period, investigations into the Hg ionization mechanism were substantially concluded. Those conclusions are summarized here. Other experiments were begun to investigate the possibilities of enhanced ionization and reduction of electrical charging. These topics will be enlarged upon in subsequent reports.

It had been suggested that during ion bombardment of (HgCd)Te, neutral Hg is preferentially evolved from the bombarded area by nonsputtering processes.² Further, Hg⁺ ions produced from (HgCd)Te by sputtering have been observed to have unusually low kinetic energies.³ These observations have suggested several experiments that could shed some light on the associated ionization phenomena.

Ion scattering spectrometry has been used to study preferential sputtering in numerous binary alloy systems.^{4, 5} We were able to obtain evidence for surface depletion of Hg by exploiting the

properties of ion scattering in a novel use of the CAMECA IMS-3f. Ion scattering is conceptually similar to the Rutherford backscattering effect in that the bombarding projectile (ion) is scattered off atoms in the target in elastic "hard sphere" collisions. Elastic collisions divide the initial momentum of the projectile ion proportionally with the masses of the projectile and the atoms in the target. Thus, the backscattered projectile ions leave with energies characteristic of the masses of the target atoms. The attractiveness of ion scattering is that the "information depth" is very shallow. In our simple experiment, the bombarding projectiles were O_2^+ ions accelerated to 8 keV of kinetic energy. This is the energy used for sputtering during routine depth profiling in the CAMECA ion probe. The recoiled O_2^+ ions were detected by sweeping the secondary extraction voltage. Peaks in the recoiled O_2^+ ion intensity at particular values of the secondary extraction voltage were then related to the atoms present in the bottom of the sputter crater. Figure 1 shows the spectrum which resulted.

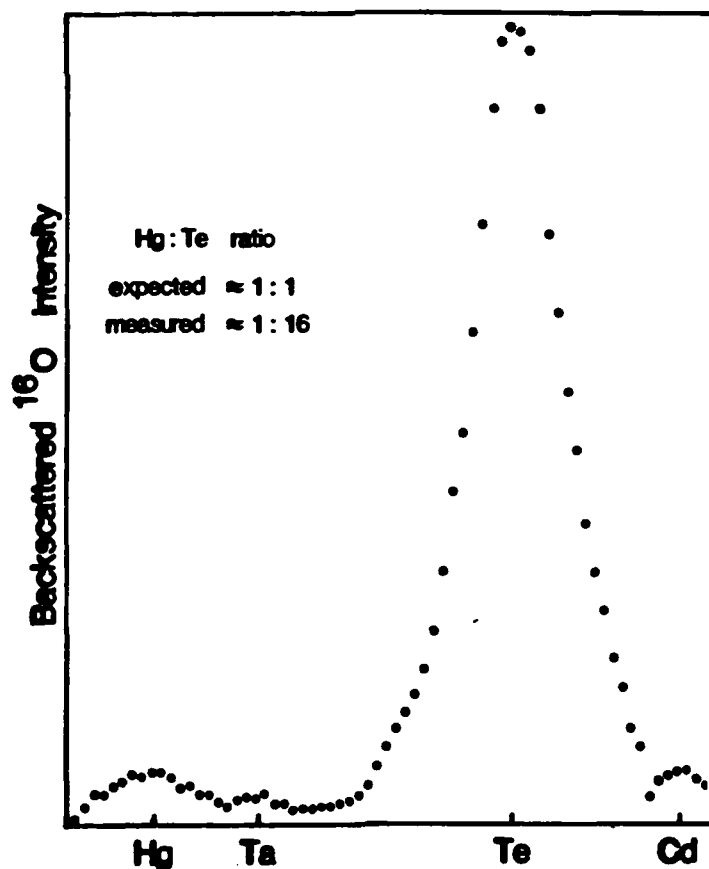


Figure 1. Ion Scattering Spectrum from (HgCd)Te

The ion scattering yield should have some nonlinear dependence on the mass, analogous to the mass squared dependence familiar to users of the Rutherford Backscattering Spectrometry technique. Even after accounting for this, the measured intensity corresponding to Hg^+ is quite low. This is in qualitative agreement with the presumption of preferential evolution of Hg.

Evidence for neutral Hg leaving the surface not as a result of sputtering (i.e. with unusually low kinetic energy) was indirect and was obtained by examining Hg^+ ion intensity versus ion kinetic energy. An example of this distribution is shown in Figure 2a. In this figure, the initial kinetic energy spread of the Hg^+ ions is superimposed on the extraction potential of 4500 eV. By comparing such a plot against a similar plot of Te^+ ion yield (Figure 2b), it became evident that a large fraction of the Hg^+ ions had less than the minimum kinetic energy that would be imparted to them by the extraction field.

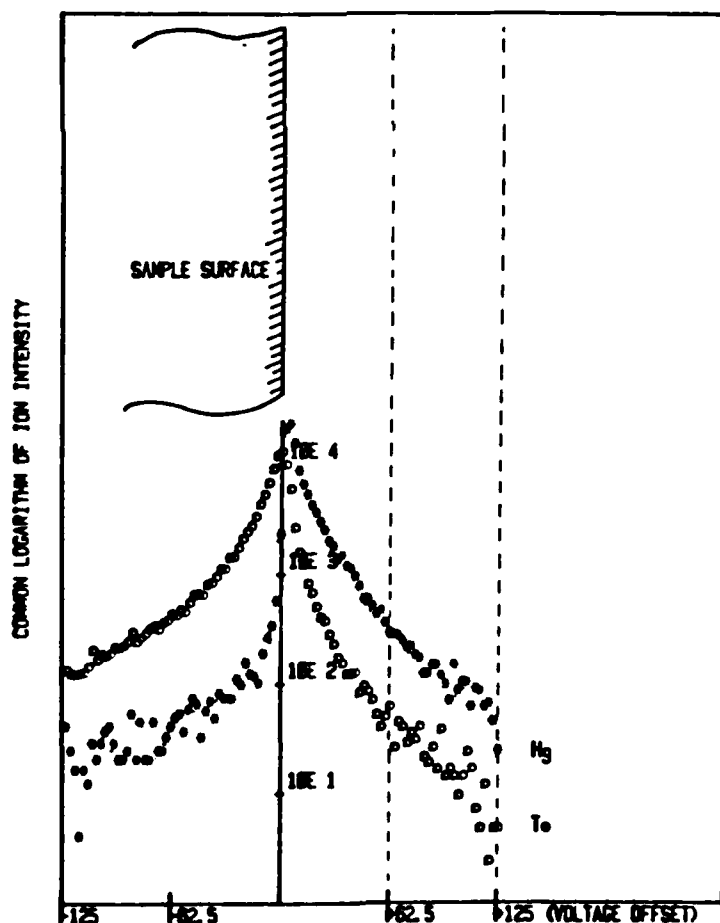


Figure 2. Hg versus Te Initial Kinetic Energy Distribution

Another experiment, this time exploiting the imaging capability of the IMS-3f gave corroborating evidence. The lateral energy of the Hg^+ ions, (the energy vector parallel to the sample surface) was observed and measured by imaging the Hg^+ signal from $(\text{HgCd})\text{Te}$ at an intermediate crossover in the ion optical path. This image was compared with Te^+ or Cd^+ lateral energy images formed in the same way. A measure of the width of the two images, corrected for different magnification factors used gave a measure of the lateral energy of 50 - 100 meV for the Hg^+ ions, in sharp contrast to the 5 - 10 eV customarily observed for sputtered ions, including Cd^+ and Te^+ . The most plausible explanation for these observations is that neutral Hg atoms must leave the bombarded surface at or near thermal energies due to local sample heating from ion bombardment.

The results presented here were obtained with the sample held at nominally room temperature. Our conclusions would be reinforced if a decrease in low energy ion yield were observed when the experiments were repeated with the sample cooled to liquid nitrogen temperature.

Thus, the question remaining to be answered: how are these low-energy Hg^+ ions formed? The proposed mechanism has to explain:

- The low energy Hg^+ ions increased approximately as a power of two with O_2^+ ion beam current density.
- If $(\text{HgCd})\text{Te}$ was bombarded with O^- , a much smaller percentage of low energy Hg^+ ions were observed.
- Simultaneous bombardment with O_2^+ and electrons or photons did not increase or decrease low energy ion production.

The most likely ionization mechanism appeared to be neutral Hg undergoing ionization by the positive oxygen primary ion beam in the vacuum above the sputtered surface.

In the CAMECA IMS-3f, the geometry of the primary beam interaction with the sputtered surface is roughly that of a cylinder intersecting with the plane of the sample at approximately a 60 degree angle. The consequence of this is a non-uniform primary beam irradiation of the volume above the sputter crater. This fact, and the ability to aperture select

ions for kinetic energy measurement from specific portions of the irradiated volume and indicated an interesting experiment to test the proposed mechanism. Thus, the experiment was to see if a large potential interaction volume would yield more low energy ions than a small interaction volume. Figure 3 shows the results of this experiment: an increase in low energy ions is realized by examining the area of greatest potential interaction.

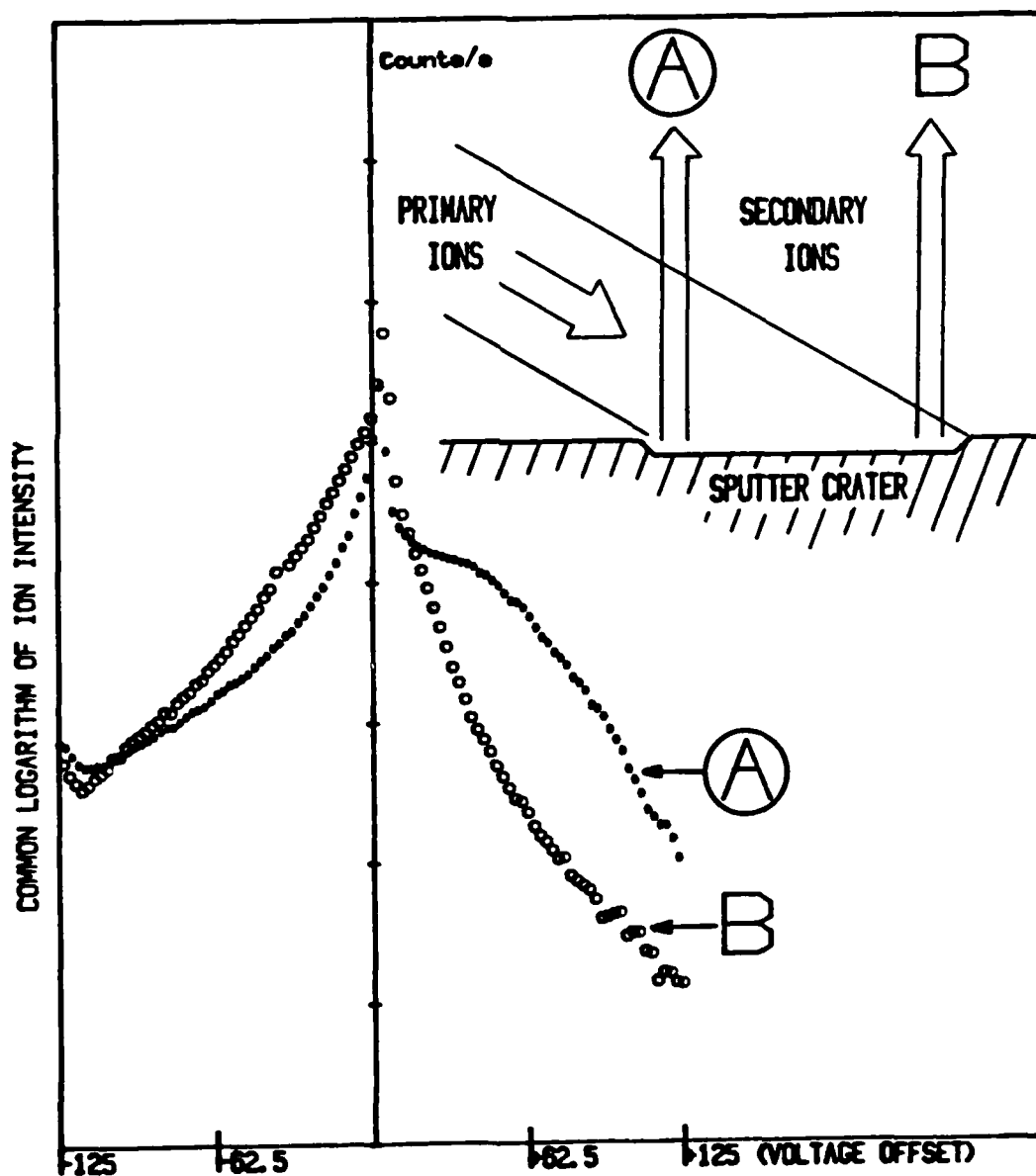


Figure 3. Evidence for Primary Beam Interaction with Neutral Hg

B. Other Analytical Techniques

Evaluation of the strengths and weaknesses with respect to the characterization of the properties of (HgCd)Te of other surface and probe type analytical tools continues as a parallel effort to that in the SIMS laboratory. In particular Auger Electron Spectroscopy (AES) and Rutherford Backscattering Spectroscopy (RBS) are presently being investigated to potentially provide information on the metal-to-(HgCd)Te bonding problems, sample morphology, crystal quality and stoichiometry.

As a first step, work has been started on determining relative sensitivity factors to be used for AES analysis of (HgCd)Te. Preliminary results look promising. RBS is being used to cross-compare the quantitation results obtained using AES. Hg can be resolved using $^4\text{He}^{++}$ (alpha particles) at the standard energy of 2.275 MeV. Higher energies (per nucleon accelerated) will be needed to resolve Cd and Te. These could be obtained by using C^+ , N^+ or O^+ beams.

C. Significant Problems / Future Work

Presently, the measured RSF's, elemental detection limits and analytical techniques apply strictly to the (HgCd)Te/CdTe system. Recently, considerable attention is being given to new compounds and substrates related to the (HgCd)Te system, such as (HgMn)Te, (CdZn)Te and other materials discussed at the recent (HgCd)Te workshop. It is clear that RSF measurements and the sputtered ion energy distribution measurements must be reconsidered to provide reliable analytical techniques for these new systems.

D. References

1. D. Betts, D. Reed, J. Huneke, K. Dimiduk, and C. Evans, Jr., Matrix and Trace Constituent Analysis in (HgCd)Te and CdTe by SIMS, Extended Abstracts for 1984 Workshop on Physics and Chemistry of Mercury Cadmium Telluride
2. H. Nitz, O. Ganshow, U. Kaiser, L. Wiedmann, and A. Benninghoven, Quasimultaneous SIMS, AES, XPS, and TDMS Study of Preferential Sputtering, Diffusion and Mercury Evaporation in $\text{Cd}_x\text{Hg}_{1-x}\text{Te}$ Surface Science, 104, L365-L383 (1981)
3. K. Wittmaack, SIMS Analysis of Cadmium Mercury Telluride, Adv. Mass Spectrometry, 8A, 503-509 (1980)
4. H. Kang, R. Shimizu and T. Okutani, ISS Measurement of Surface Composition of Au-Cu Alloys by Simultaneous Ion Bombardments with Ar and He Ions Surface Science, 116, L173-L178 (1982)
5. T. Okutani, M. Shikata and R. Shimizu, Investigation on Surface Compositions of Cu-Ni Alloy Under Ar Ion Bombardment by ISS and In-Situ AES Measurements Surface Science, 99, L410-L418 (1980)

MeV Ion Implantation Studies At Charles Evans & Associates

Introduction

The study of high energy ion implantation (MeV implants) at CHARLES EVANS & ASSOCIATES was initiated to support the research effort under DARPA contract #MDA903-82-C-0427. The goal of this research is to characterize the material properties and to develop new analytical methods for the compound semiconductor mercury cadmium telluride (MCT). One of the major needs in the characterization of MCT is the quantitation of the many impurities which are often unintentionally incorporated into the material. For the purposes of this study Secondary Ion Mass Spectrometry (SIMS) was chosen as the primary analytical technique for investigating the residual trace impurities in MCT.

It has been previously shown (1-4) that the secondary ion yield for a given impurity atomic species is a strong function of the matrix (or substrate) in which the impurity atom is present. This "matrix effect" poses a severe problem when SIMS is used for the quantitation of impurities a new, unstandardized material. However, this apparent problem can easily be circumvented by experimentally establishing the secondary ion yield for a given impurity-matrix combination to yield a Relative Sensitivity Factor (RSF). Once the RSF has been established it can be used to accurately calculate an impurity concentrations which may vary over many orders of magnitude (5). The typical method used to establish an RSF is to perform a SIMS analysis on a sample or a set of samples which have known impurity concentrations. For silicon-based technology there are several different methods available for preparing these "standards" which are used to compute the RSF.

The first method of preparing SIMS standards for silicon dopants is to incorporate the impurity during the crystal growth process. That is, a known amount of the impurity can be added to the "melt" from which the crystal is to be pulled. However, the most common method of preparing a "SIMS standard" is to ion-implant the impurity into the matrix of interest. This method is particularly useful when there is no way to prepare a sample by bulk doping. The ion implantation process produces a uniformly doped sample with an accurate concentration of the desired impurity (6). If the dopant is of the type which become electrically active when substitutional in the crystal

lattice, then the concentration can also be cross-checked by electrical measurement techniques.

High performance SIMS analysis employs a reactive ion such as oxygen or cesium to bring about the sputtering process. These chemically reactive atoms are implanted in the near surface of the sample and enhance the production of either positive or negative secondary ion depending on whether oxygen or cesium bombardment is used. The practice of reactive ion sputtering increases the ultimate detection limits of the SIMS technique by several orders of magnitude over the use of non-reactive ion sputtering (7).

To investigate conventional ion implantation into MCT, several samples were ion-implanted and subsequently analyzed by SIMS. The SIMS analysis revealed, as expected, that the implantation depth was extremely shallow in the "high Z" matrix of MCT. Shallow implantation was the case for even the highest energies obtainable from the conventional ion implanter. That is, due to the high atomic number of the MCT matrix, the stopping power of MCT is much greater than that of silicon, the material for which conventional ion implantation systems are optimized. For many implanted elements the near surface region of MCT often had a high concentration of residual impurities (8). The convolution of the profile from the surface impurity and that due to the shallow depth of implantation for conventional ion implantation caused some difficulties in obtaining good quantitation of the implant. This suggested that higher energy ion implantation given greater depth of penetration might be useful for the production of SIMS quantitation standards for MCT.

Many applications for megaelectron volt (MeV) ion implantation have recently been proposed (9-10), however, these papers point out that there is presently very little experimental data to support the physical phenomena relating to MeV implantation. Thus we felt it prudent for the first set of experiments to investigate MeV implantation into the more conventional and better understood single crystal silicon materials system.

Experimental Design

As stated, the first set of experiments on MeV implants were designed using silicon as the implant substrate. The choice of silicon as the substrate for the initial experiments allows the large volume of knowledge about implantation into silicon to act as a guide when unexpected observations are

made. In this way, if unusual results are obtained in the course of the experiment, there is a good data base from which to detect potential experimental errors. This is particularly the case when moving from the well characterized system of silicon into the much less understood materials systems presented by the compound semiconductors such as MCT.

The implants used in this preliminary study were performed by Dwane Ingram at Universal Energy Systems of Dayton, Ohio. Implants of both boron and phosphorous were performed into <111> silicon at 0.8, 1.2, and 2.0 MeV. One implant with the sample tilted at 7 degrees with respect to the beam was performed at each energy. A second sample tilt angle was implanted at 1.2 MeV for both of the dopants used in this study. For the case of the boron implants, a portion of each of the as-implanted wafers was annealed and both the as-implanted and annealed samples were analyzed. For the phosphorous implants, different as-implanted and annealed wafer sets were analyzed to help study the machine repeatability and accuracy from day to day. The sample set for this study is shown in Figure 1. As a point of reference SIMS depth profiles and Rutherford backscattering spectra taken from conventional boron and phosphorous implants are shown in Figures 2 and 3. The discussion will proceed first to the study of the boron-implanted samples and then to the phosphorous-implanted samples.

MeV Boron Implantation into Silicon

The first measurement performed was to check the implantation dose accuracy for each of the as-implanted and annealed samples. The results of this SIMS analysis is shown in Figure 4. Note that all of the SIMS dose measurements are somewhat lower than the projected dose of 1×10^{14} atoms/cm². For all of the samples which were implanted at the 7 degree tilt, the absolute dose error as measured by SIMS is less than 14 percent. This figure is well within the accuracy of conventional high dose ion implanters (11). The dose error for the sample which was tilted 52 degrees with respect to the beam, is considerably greater than those implanted at a 7 degree tilt. However, if the measured dose is corrected for the inverse cosine relation of the area of the sample intercepted by the beam at this large tilt angle, then the measured dose error becomes less than 3 percent (a figure which is better than the expected experimental error in the SIMS measurement). For all of the samples the as-implanted dose agrees very well with the measured dose after annealing. This is consistent with results which are obtained when similar

annealing conditions are used for conventional boron-ion implants.

The second analysis was to measure the boron range in each of the samples. The data shown in Figure 5 indicates that there is a shift in the peak of the concentration (mean depth as measured using SIMS) shifting toward the surface of each of the annealed samples. The SIMS depth profiles, from which this range data was measured, is shown in Figure 6. The apparent diffusion towards the surface of the sample may be just that, an enhanced movement of the boron during annealing into the damage region produced near the end of range for the implanted ions. See reference 4 for a more detailed description of the end-of-range damage phenomena. Figure 5 also shows the mean depth of the electrical activity in the annealed samples. The spreading resistance measurements were performed by the staff of Universal Energy Systems. We presently do not have a theory for why the electrical activity is peaked at a much more shallow depth than the atomic concentration.

Of the depth profiles shown in Figure 6, the profile for the as-implanted 1.2 MeV/7 degree tilt sample is particularly interesting. The depth distribution of the boron in this sample has a very non-standard profile. After the normal peak in the concentration at 2.03 micrometers there is a second smaller peak at 2.2 micrometers. There are several possible explanations for the existence of this second peak. Most of them, such as multiple energy implants, or molecular disassociation (16), can be discarded because of the experimental procedure which was used for these implants. A second anomaly is revealed when the boron range in the 1.2 MeV/52 degree tilt as-implanted sample is compared to the LSS projected range (17) for a sample with this orientation. Figure 7 shows the comparison of each of the experimentally observed concentration maxima in the 0.8 and 1.2 MeV boron-implanted samples with the LSS projected range for these sample orientations and beam energies. Note that the range, as determined by SIMS, is in very good agreement with the LSS theory for the 0.8 MeV/7 degree tilt and the first maxima in the 1.2 MeV/7 degree tilt. There is a considerable disagreement between the 1.2 MeV/52 degree tilt and the second peak in the 1.2 MeV/7 degree and the LSS projected range for these sample orientations and ion energies.

The question arises as to the relationship between the anomalously deep peak concentration in the 1.2 MeV/52 degree sample and the anomalously deep second peak in the 1.2 MeV/7 degree sample. The solution to this question is diagramed in Figure 8. Here it is shown that, if the depth at which the

maximum concentration of the boron in the 1.2 MeV/52 degree sample is projected onto the 1.2 MeV/7 degree sample, this maximum concentration very closely matches the depth at which the second peak occurred. This observation suggests that the 1.2 MeV/52 degree range may be due to channeling of the beam during the implantation process. After this observation it was found that the original $\langle 111 \rangle$ wafers which were used for the substrates did not have any flats ground on to the wafer perimeter. This means that there was no way of properly orienting the wafers prior to implantation to minimize channeling effects. The RBS data shown in Figure 9 indicates that little damage was done to the crystal during the implantation process. This is demonstrated by the fact that the channeled spectra of the as-implanted sample is very similar to a virgin $\langle 111 \rangle$ silicon slice.

This hypothesis can explain the "too deep" implant depths. It does not address the issue of why implant depths corresponding to both channeled and random orientations are observed in the same sample. Possible explanations for this observation include: 1) that the overall beam divergence is relatively large so that only that portion of the beam which has a divergence less than the half angle will be channeled, or 2) that the beam angle with respect to the sample changed during the course of the implant. Neither of these two explanations is entirely satisfactory. In the case of a beam with a fairly large divergence there is not a well defined "cut-off" function which would account for separation of the beam into channeled and non-channeled fractions. In the case of the sample/beam angle changing, the system used to implant these samples electrostatically scans the beam across the wafer surface. This type of system can cause changes in the beam/wafer angle macroscopically across the wafer (12). The analytical region used for this analysis was approximately a 100 micrometer square area. It is difficult to envision a method by which the scan system could change the beam/sample angle sufficiently to create distinct channeled and random orientations within this small an area. At the time of this report several other possible explanations are being investigated. These topics will be covered in the section on continuing research.

An additional observation can be made once the concept of the beam being split into channeled and random fractions is proposed. This observation is shown in Figure 10. By the vivid use of one's imagination, numerous "fractions" can be observed in all of the MeV boron implants. By careful reexamination of the conventional implant used as the SIMS standard, a shoulder can also be

observed in the data presented in Figure 2. Perhaps this phenomenon also exists in low energy ion implantation into silicon but the separation between the different peaks is insufficient to allow them to be observed. Only by increasing the beam energy, and thus the range of the particles, can the multiple range peaks be separated sufficiently for detection by the SIMS technique. As previously stated, more investigation into this phenomenon is warranted.

MeV Phosphorous Implantation

The choice to use samples from different implanter runs for the as-implanted and annealed samples preclude the ability to check for "dose outgassing" and diffusion during the annealing process. This is shown in Figure 11. If the dose for the sample tilted 52 degrees, with respect to the beam, is corrected for the increased area which is intercepted by the beam, then the experimentally measured implanted dose for the as-implanted samples are all grouped around $8E13$ atoms/cm². Similarly, the annealed samples are all grouped around $5.5E13$ atoms/cm². Because the same sample was not used in the annealing study it is impossible to determine if the discrepancy in dose is due to the annealing or due to a change in the calibration of the dose monitoring equipment on the ion implanter.

This is also the case in attempting to determine if diffusion had occurred during the anneal. Figure 12 shows the depth of the peak concentration as determined by both SIMS and SRP. There is an "apparent" diffusion towards the surface of the sample in the three lower energy samples and an "apparent" indiffusion in the sample implanted at 2 MeV. Due to the fact that the as-implanted and annealed samples are potentially from two separate implants, no conclusion can be drawn from this observation. The next round of experiments will include a coherent set of as-implanted/annealed phosphorous implanted samples. One interesting observation can be made from the annealed samples by comparing the SIMS versus the SRP data. Note that as the implant energy is increased, the difference between the peak of the electrically active phosphorous and the actual phosphorous concentration becomes greater. Recall that this is similar to the case of the boron implants.

Note that there are not any pronounced multiple peaks in any of the phosphorous as-implanted samples (Figure 13). There are at least two possible explanations for this including: 1) the ΔR_p is larger than the distance

between the peaks and 2) that the crystal was sufficiently damaged that channeling effects were reduced. It is clear from the SIMS profiles of the boron and phosphorous implants that the range straggling (ΔR_p) is much greater for the phosphorous implants. Figure 14 is a comparison of the RBS channeled spectra obtained from the 1.2 MeV/52 degree tilt sample and a virgin $\langle 111 \rangle$ silicon wafer. Note that the MeV implanted sample shows a considerable amount of dechanneling as compared to the unimplanted sample and that the dechanneling increases near the end of range for this particular implant.

Summary and Proposed Experiments

The dose accuracy of MeV boron implantation into $\langle 111 \rangle$ silicon appears to be comparable to that of conventional boron ion implantation. The case for phosphorous is not as clear. For the two cases, annealed and as-implanted the implanted dose was from 20 to 45 percent different than the projected total ion dose. This may cause a problem if this technique is to be used to generate standard samples for the computation of relative sensitivity factors for SIMS. In the case of boron, the depth distribution of this particular dopant may be very sensitive to the orientation of the implant beam with respect to the crystal substrate during the implantation process. In particular, multiple dopant concentration peaks were observed in a silicon $\langle 111 \rangle$ substrate upon completion of a single ion implantation step. In an effort to better understand and repeat this finding the following experiment is proposed.

A new very thin (approximately 1 micrometer) silicon target sample will be generated so that a surface barrier detector can be placed in a transmission mode behind the sample. This sample can be generated by boron diffusing a standard n-type silicon wafer so that the diffusion depth is one micron. The wafer can then be backside-etched with an acid which will stop when the p-type boron doped layer is reached. This technique has been used by several different authors to produce foils of greater than 2 centimeters in diameter (13-14). A megavolt helium ion would then be focused on to the foil with the detector behind the foil. The sample could then be tilted through channeling and random orientations. If fractions of the beam become channeled, then the energy loss experienced by these fractions would decrease with respect to the unchanneled beam. This "dynamic" type of beam fractionation detection would be much quicker than implanting multiple sample orientations and subsequent SIMS analysis on each of the resulting samples. It is the belief of this

author that the multiple peaks observed in the boron-implanted samples are related to the "blocking patterns" (15) which can be observed under MeV helium ion irradiation when a florescent screen is placed behind one of these thin single crystal films and the film is subsequently tilted through different angles.

Conclusion

MeV ion implantation may prove to be an acceptable method of producing trace impurity standards for MCT. However, in the course of the above work some interesting questions arose even in the much more mature materials system of single crystal silicon. These questions will need to be addressed before MeV ion implantation can be used as a viable method for the generation of RSF's for secondary ion mass spectrometry analysis of the compound semiconductor, mercury cadmium teluride.

Literature Cited

1. "High Mass Resolution Secondary Ion Mass Spectrometry," P. Williams and C. A. Evans, Jr., NBS Spec. Publ. 427, Workshop on Secondary Ion Mass Spectrometry (SIMS) and Ion Microprobe Mass Analysis held at NBS, Gaithersburg, Maryland, September 16-18, 1974 (Issued October, 1975).
2. "Evaluation of the Local Thermal Equilibrium Model 101 Quantitative Secondary Ion Mass Spectrometric Analysis," D. S. Simons, J. E. Baker and Charles A. Evans, Jr., Analytical Chemistry, Vol. 48, page 1341, August 1976.
3. "Mechanism of the SIMS Matrix Effect," V. R. Deline, W. Katz and C. A. Evans, Jr., Applied Physics Letters, 33(9), November 1, 1978.
4. "Modern Ion Beam and Related Techniques for Materials Characterization," R. J. Blattner and C. A. Evans, Jr., Crystal Growth, A Tutorial Approach, W. Bardsley, D. T. J. Hurle and J. B. Mullin (eds), North-Holland Publishing Company, 1979.
5. "Factors Influencing Secondary Ion Yields," V. R. Deline, Proceedings of SIMS II, pp. 48-52 (1979).
6. "Quantitative Aspects of Secondary Ion Mass Spectrometry," V. R. Deline (1978) [thesis].
7. "High-Performance Secondary Ion Mass Spectrometry," R. J. Blattner and C. A. Evans, Jr., SEM, INC., Chicago, Illinois, O. Jahari, ed. (1980).
8. "Characterization of Impurities in HgCdTe by SIMS," Review of Defense Advanced Research Projects Agency, Defense Sciences Office, Focal Plane Materials Research Program, December 1-2, 1982.
9. "MeV Implantation in Semiconductors," N. W. Cheung, SPIE Proceedings, Vol 530, 1985.
10. "MeV Implantation for Silicon Device Fabrication," D. Pramanik and M. I. Current, Solid State Technology, May, 1984.

11. "Materials Characterization Tools for Advanced Ion Beam Processes," M. D. Strathman, SPIE Proceedings, Vol 530, 1985.
12. "Improved Uniformity of Implanted Dose by a Compensated Scan Pattern Generator," N. Turner, Nuclear Inst. & Methods, Vol. 189, 1981, p. 311-318.
13. "Thin Silicon Foils," N. Cheung, Rev. of Scientific Inst., Vol. 51, 1980, p. 1212.
14. Charles Slayman, Hughes Research Laboratories, Malibu, California, private communication.
15. "Blocking Effects in the Emergency of Charged Particles from Single Crystals," D. S. Gemmell and R. E. Holland, Physics Review Letters, 14(23):945-8, 1965.
16. "Anomalous Boron Profiles Produced by BF₂ Implantation into Silicon," T. W. Sigmon, V. R. Deline, C. A. Evans, Jr. and W. M. Katz, Journal of the Electrochemical Society, Vol. 127, No. 4, April 1980.
17. "Projected Range Statistics, Semiconductors and Related Materials," J. F. Gibbons and S. W. Mylroie, Dowden, Hutchinson & Ross, Inc., 1975.

Figure Captions

Figure 1

Description of the samples discussed in this paper.

Figure 2

Secondary ion mass spectrometry depth profiles of conventional ion-implanted boron and phosphorous into silicon. These samples are the standards used to calibrate the dose measurements presented in this work.

Figure 3

Rutherford backscattering spectra of the samples presented in Figure 2. The spectra were obtained using both the channelled and random orientation of the sample with respect to the beam in order to show the damage caused to the single crystal substrate in a conventional ion implantation process.

Figure 4

Dose accuracy of the boron MeV ion implants, a comparison of as-implanted and annealed samples.

Figure 5

A comparison of the mean depth of the boron concentration as determined by SIMS before and after the annealing process. Also shown is the mean depth as determined by spreading resistance profiling.

Figure 6

The secondary ion mass spectrometry depth profiles for the MeV boron ion implanted samples. Both the as-implanted and annealed samples are depicted.

Figure 7

A comparison of the mean depth of the MeV ion implants and the range which is projected using LSS theory. Note the secondary peak in the spectra obtained from the sample implanted at 1.2 MeV with a sample tilt of 7 degrees.

Figure 8

Schematic of the effect of sample tilting on the implantation depth. Also, a projection of mean implantation depth measured from the 52 degree sample on to the sample which was tilted 52 degrees with respect to the beam.

Figure 9

A set of Rutherford backscattering spectra which show that the damage generated in the MeV boron-implanted sample is minimal.

Figure 10

Schematic drawing which depicts possible multiple peaks in the SIMS profiles obtained from the MeV boron ion-implanted samples.

Figure 11

Dose accuracy of the phosphorous ion-implanted samples as determined by SIMS.

Figure 12

Comparison of the mean phosphorous concentration before annealing as determined by SIMS and after annealing by both SIMS and SRP.

Figure 13

Secondary ion mass spectra obtained from the MeV phosphorous ion-implanted samples.

Figure 14

Channelled RBS spectra of the MeV phosphorous ion-implanted samples.

DESCRIPTION OF SAMPLES

ENERGY (MeV)	ANGLE (DEG.)	BORON IMPLANTS	
		Sample Identification	
		AS IMPLANTED	ANNEALED
0.8	7	0321-1511-3	0321-1511-3
1.2	7	0321-1512-1	0321-1512-1
1.2	52	0321-1512-2	0321-1512-2
2.0	7	0321-1512-3	0321-1512-3

PHOSPHORUS IMPLANTS			
ENERGY (MeV)	ANGLE (DEG.)	AS IMPLANTED	ANNEALED
0.8	7	0321-1515-3	304-1220-3
1.2	7	0321-1514-1	304-1218-1
1.2	52	0321-1514-2	304-1218-2
2.0	7	0321-1517-1	304-1218-3

Argon anneal at 550 Deg C for 1 hr, ramp to 850 Deg C, hold for 1/2 hr

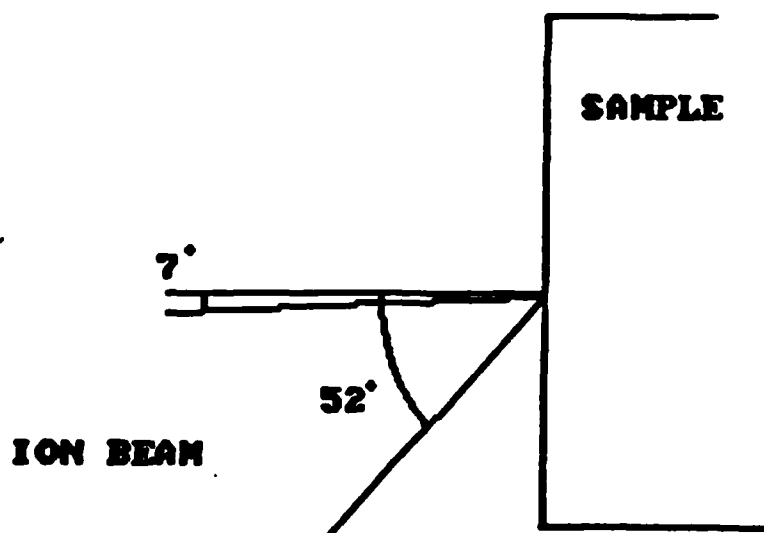
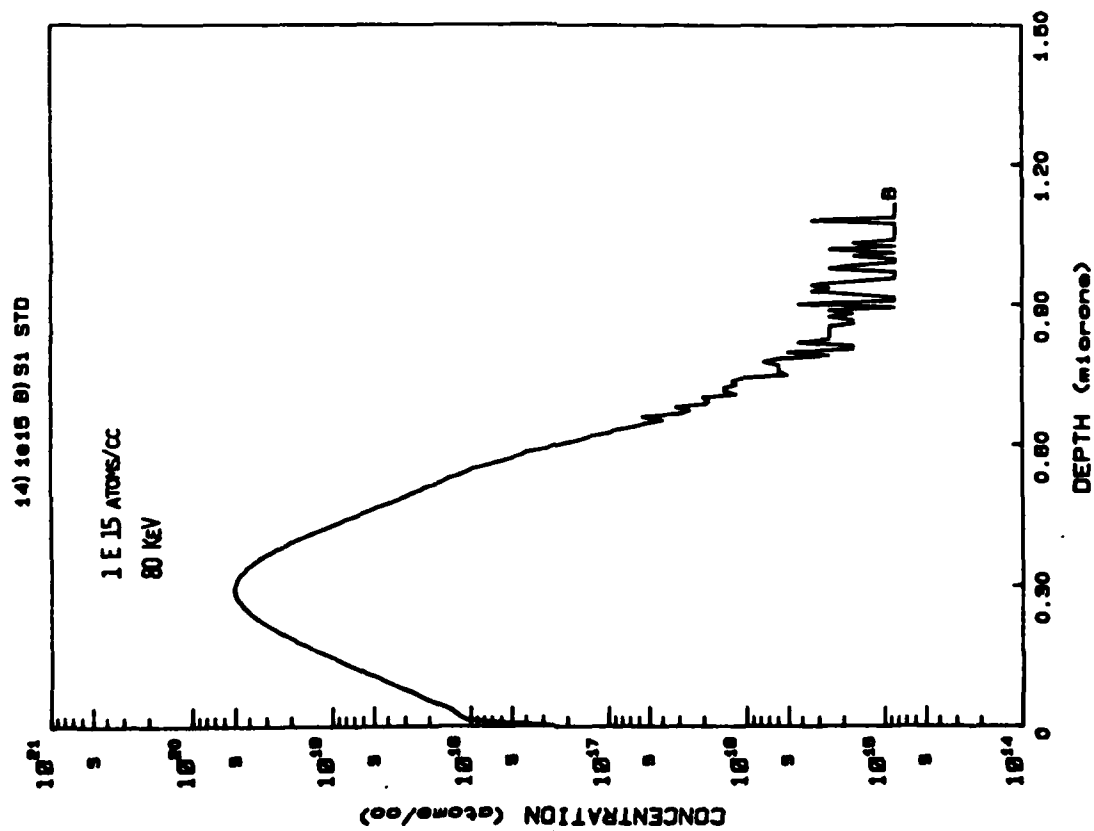


Figure #1

PROCESSED DATA

CHARLES EVANS & ASSOCIATES 10-22-84 DEPTH PROFILE



PROCESSED DATA

CHARLES EVANS & ASSOCIATES 10-10-84 DEPTH PROFILE

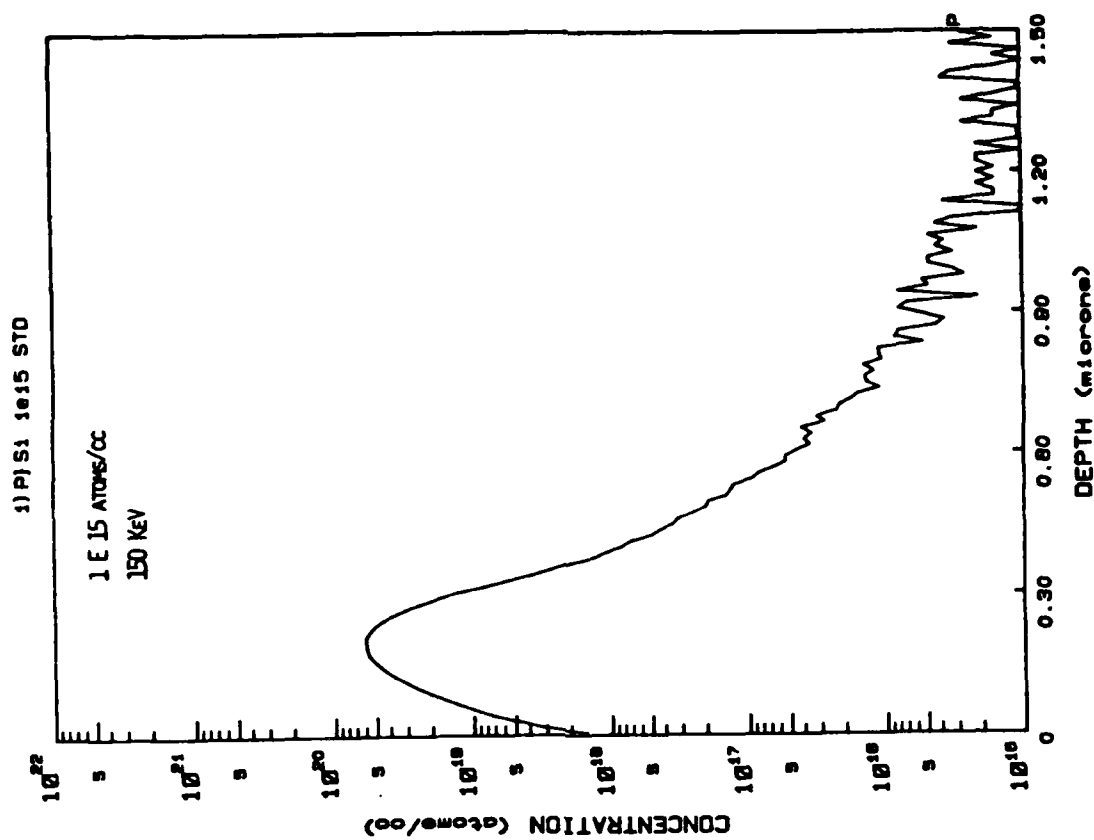


Figure #2

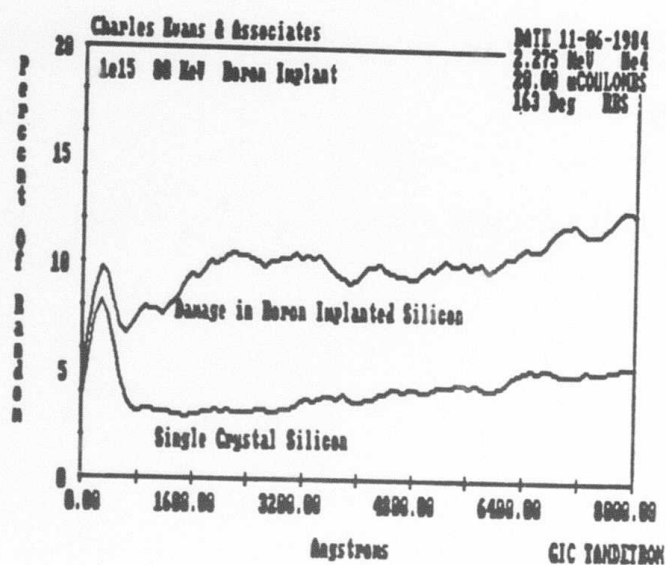
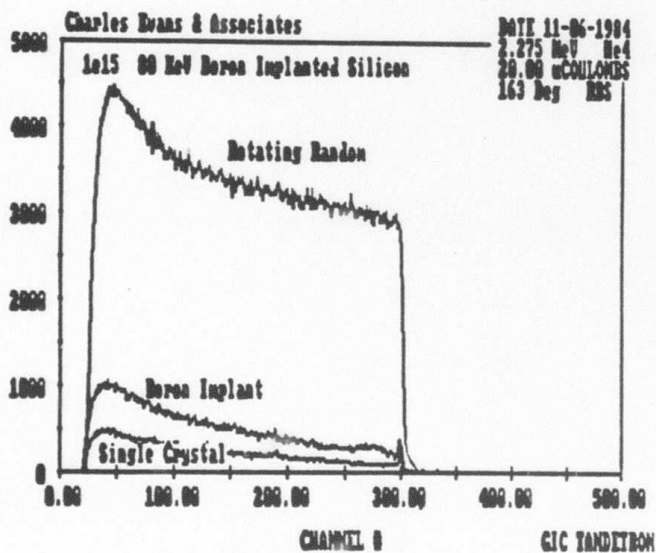
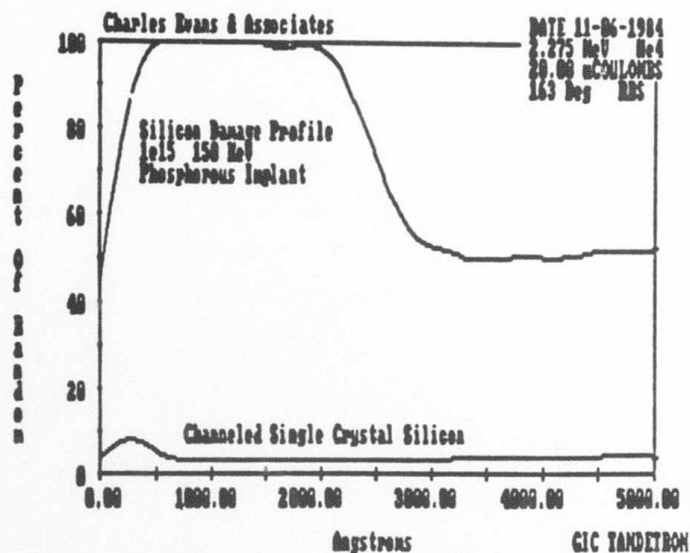
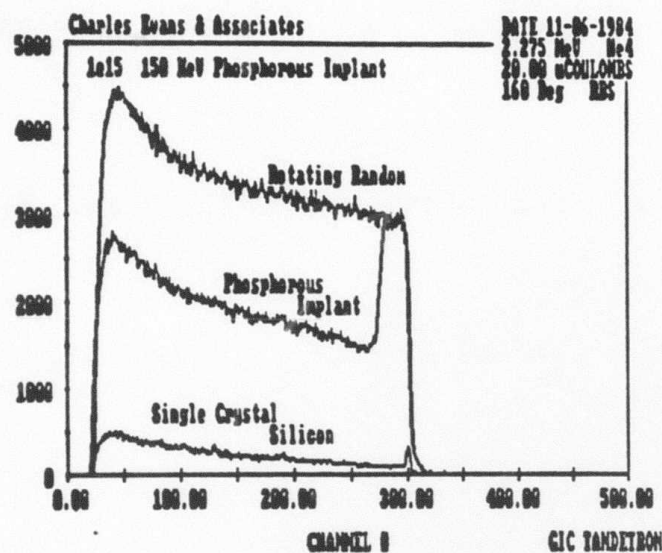


Figure #3

Total Integrated Processed Counts

Sample	As Implanted	Annealed	Nominal Dose	
			As Implanted	Annealed
800KeV 7° B #0321-1511-3	1.2E20	1.2E20	8.6E13	8.6E13
1.2MeV 7° B #0321-1512-1	1.3E20	1.3E20	9.9E13	9.9E13
1.2MeV 52° B #0321-1512-2	8.5E19	8.6E19	6E13	6.2E13
2.0MeV 7° B #0321-1512-3	1.2E20	1.2E20	8.6E13	8.6E13

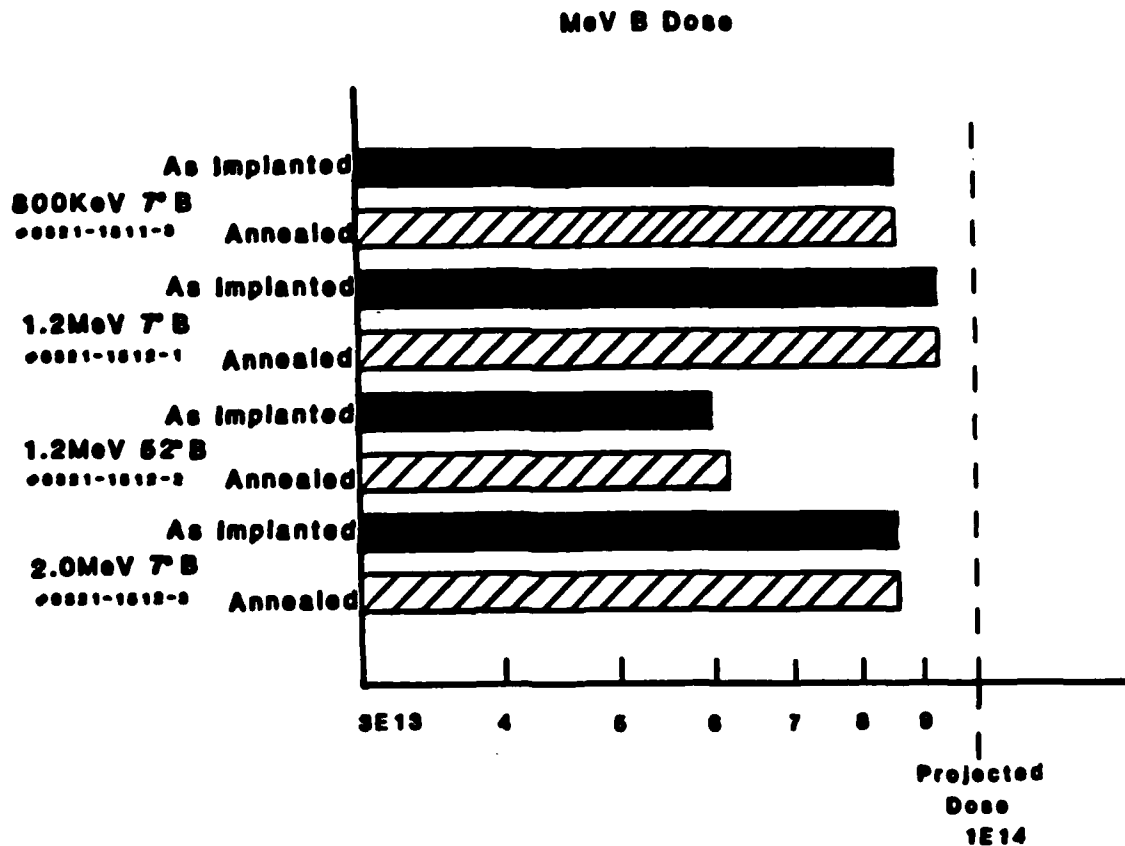


Figure #4

MEV BORON IMPLANT MEAN DEPTH IN MICRONS

IMPLANT CONDITIONS	SIMS AS-IMP	SIMS ANNEALED	SRP
0.8 MEV 7 DEGREES	1.47	1.47	1.35
1.2 MEV 7 DEGREES	2.03	2.00	1.98
1.2 MEV 52 DEGREES	1.38	1.33	1.08
2.0 MEV 7 DEGREES	2.93	2.88	2.54

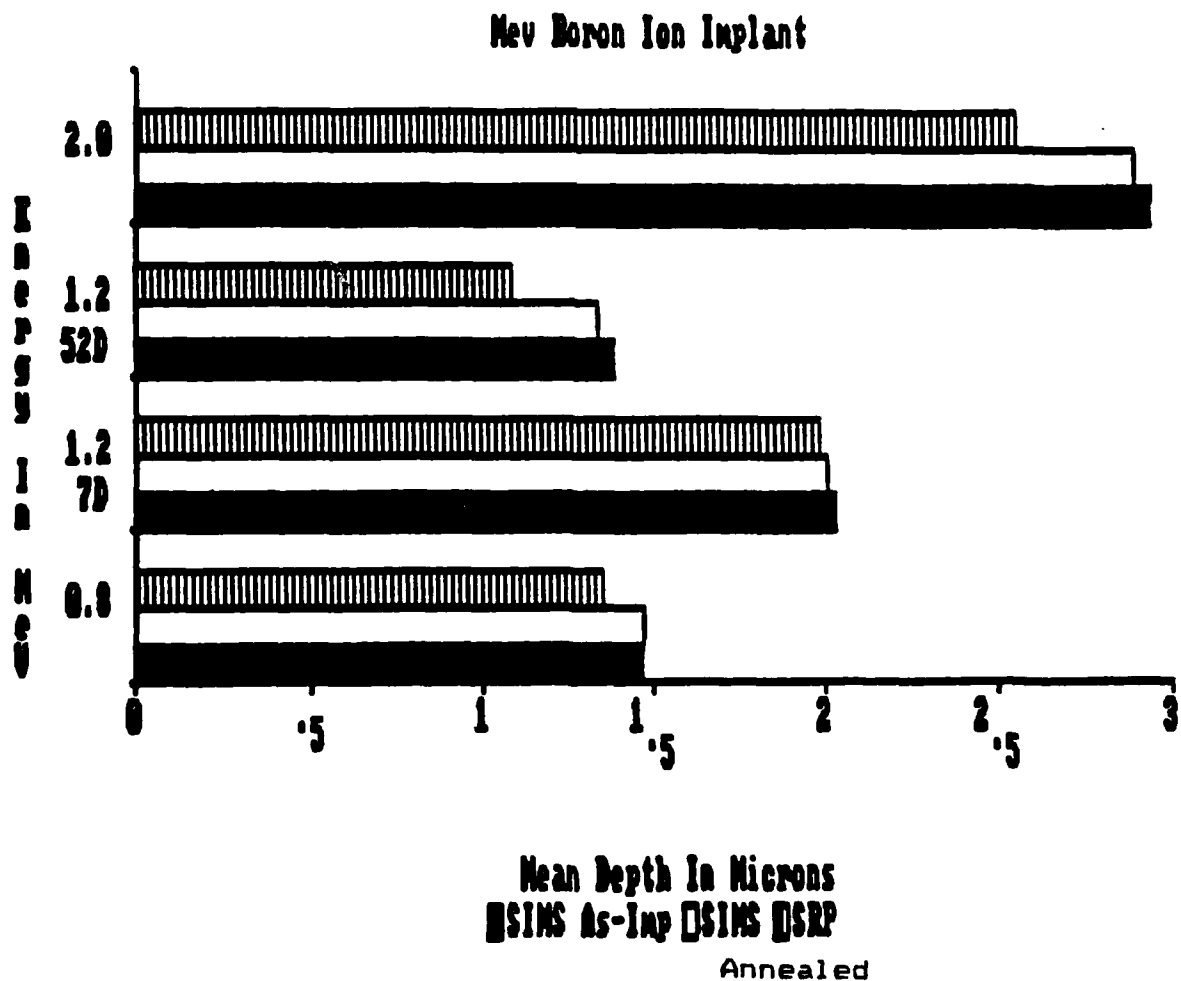


Figure #5

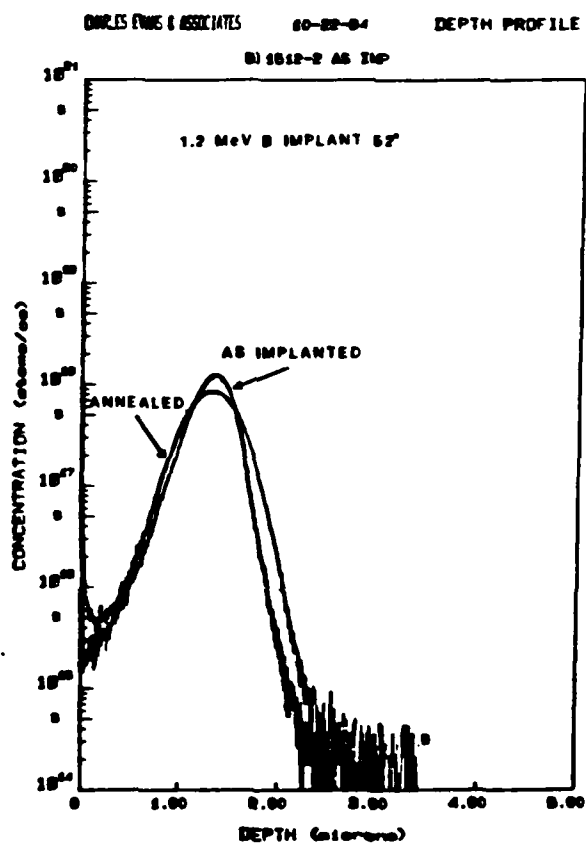
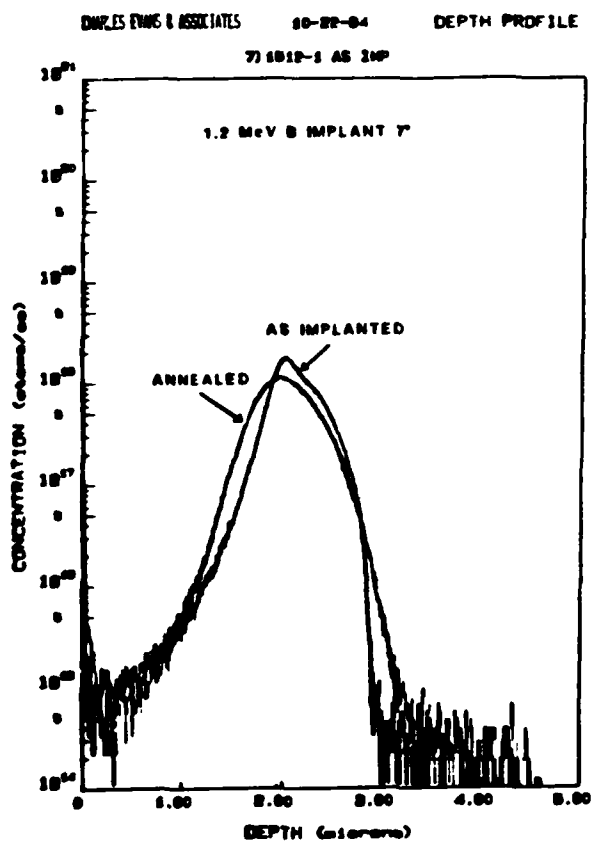
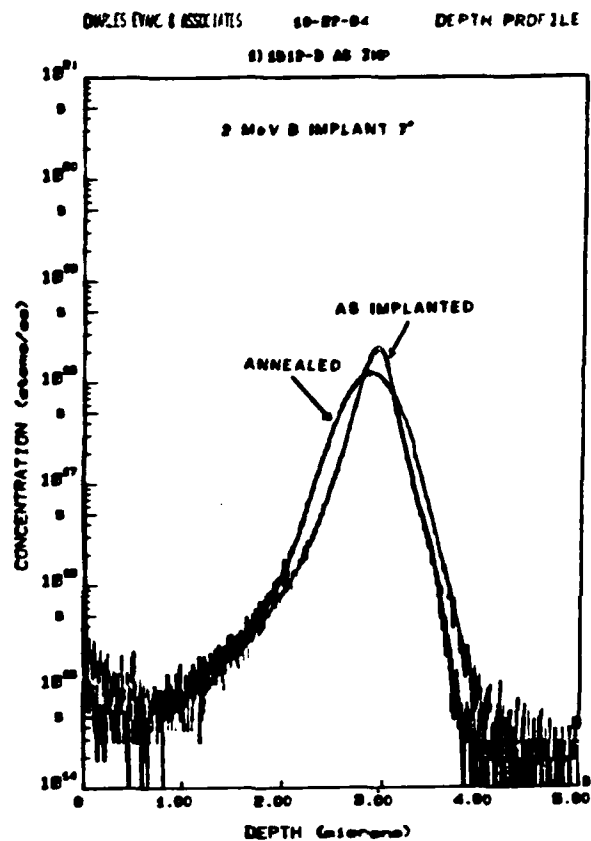
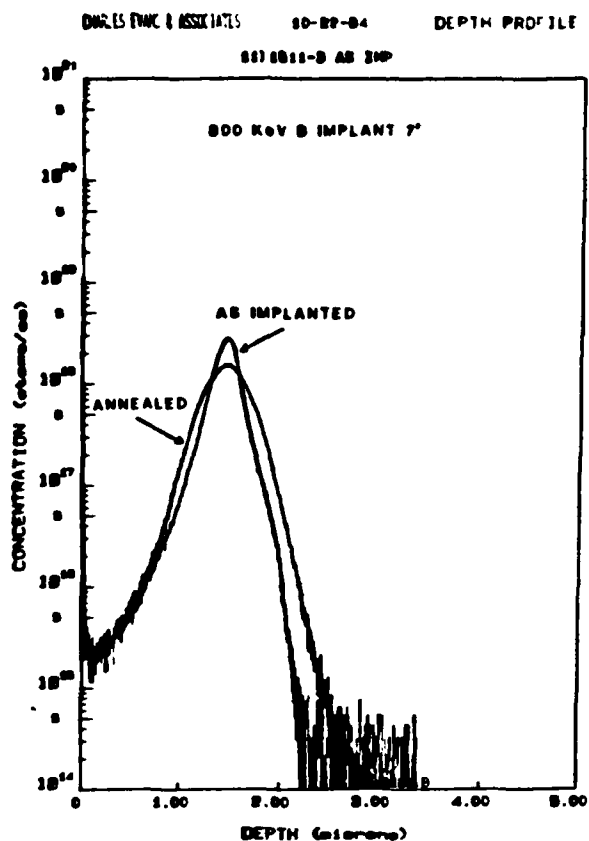
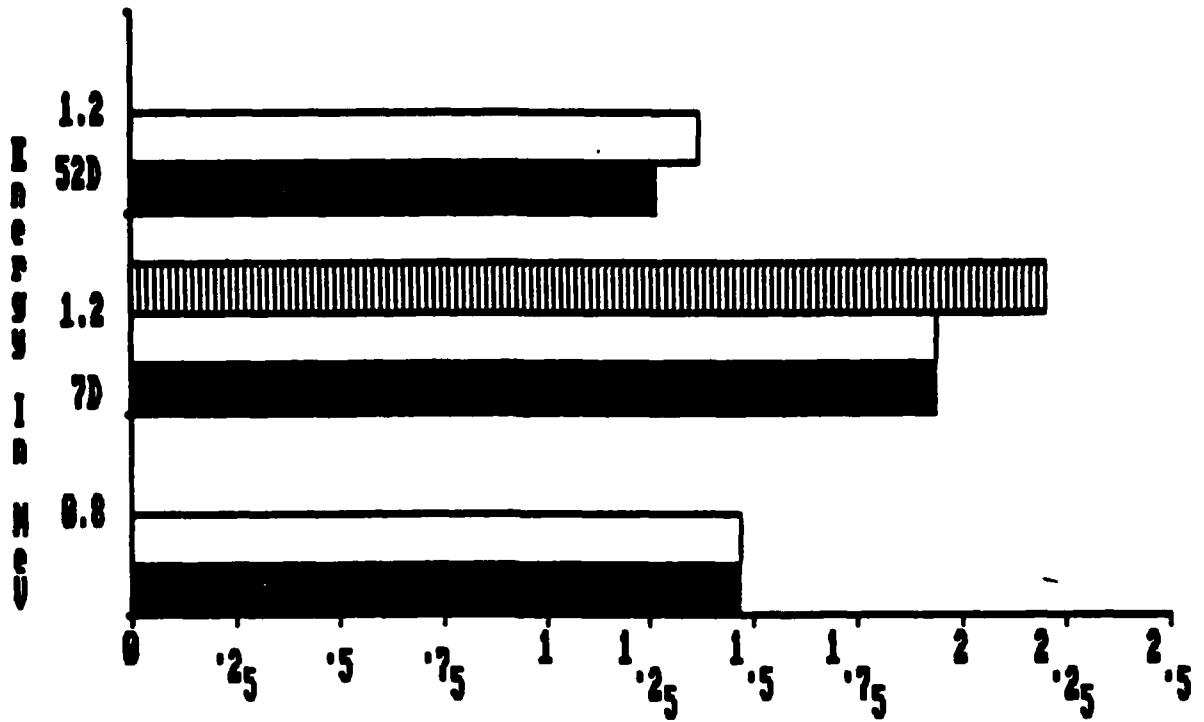


Figure #6

Projected Range vs SIMS Measured Depth



Mean Depth In Microns
 ■ Projected Range □ SIMS Peak #1 ▨ SIMS Peak #2

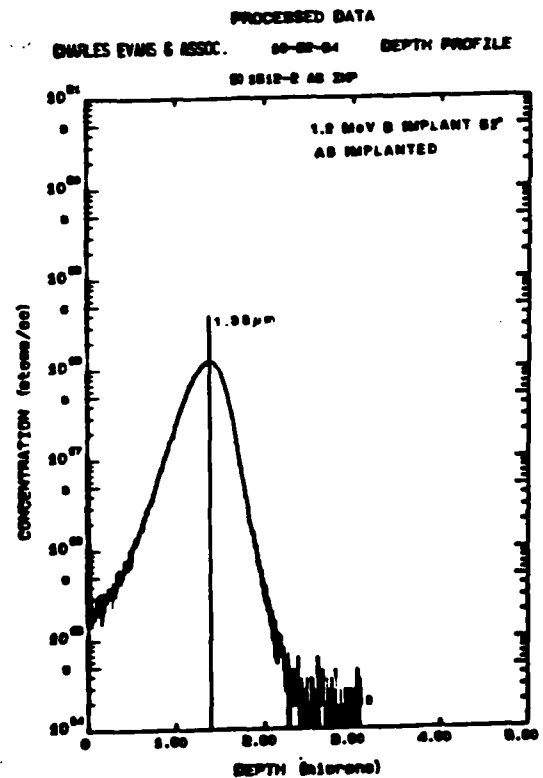
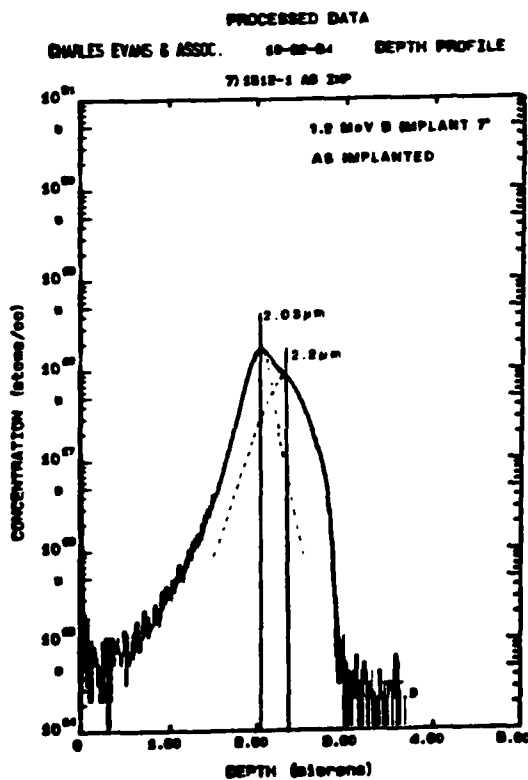
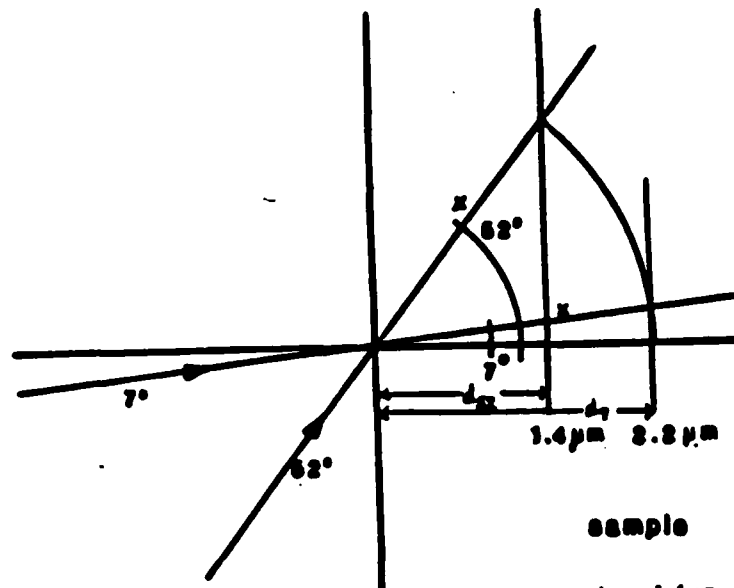


Figure #7

Effect of Beam Incident Angle on Implant Depth



So, if we assume $d_{52} = 1.4 \mu\text{m}$, then

$$d_1 = \frac{\cos 7^\circ}{\cos 52^\circ} \cdot 1.4$$

$$d_1 = 2.2 \mu\text{m}$$

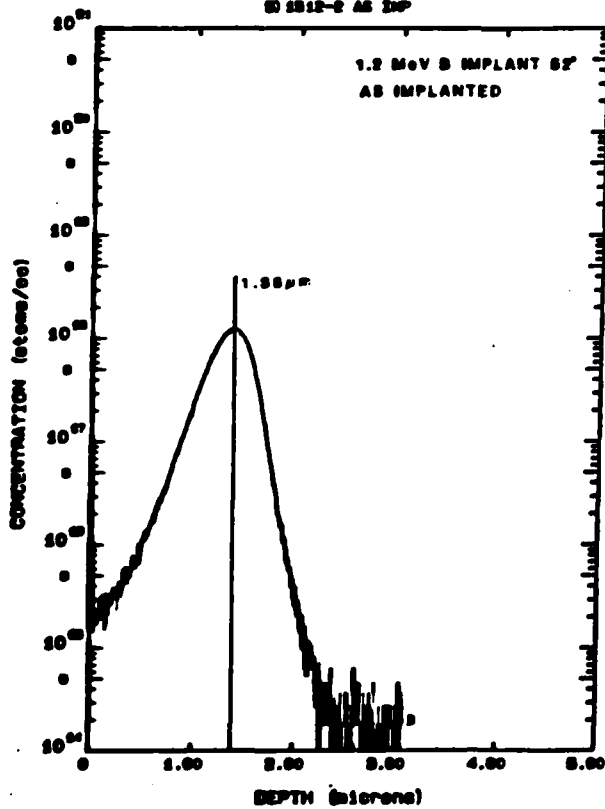
$$\cos 7^\circ = \frac{d_1}{x} \Rightarrow x = \frac{d_1}{\cos 7^\circ}$$

$$\cos 52^\circ = \frac{d_{52}}{x} \Rightarrow x = \frac{d_{52}}{\cos 52^\circ}$$

PROCESSED DATA

CHARLES EVANS & ASSOC. 10-02-84 DEPTH PROFILE

77 1012-2 AS 3DP



PROCESSED DATA

CHARLES EVANS & ASSOC. 10-02-84 DEPTH PROFILE

77 1012-1 AS 3DP

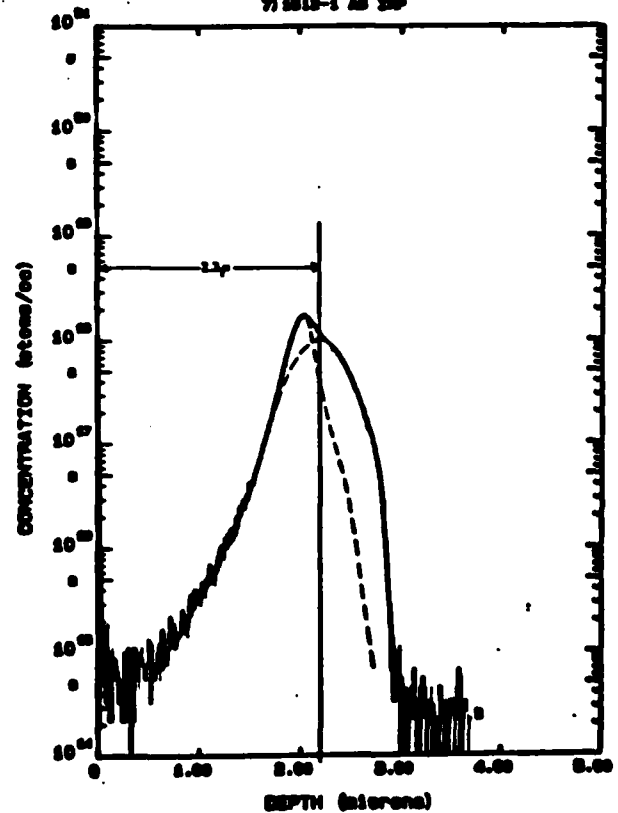
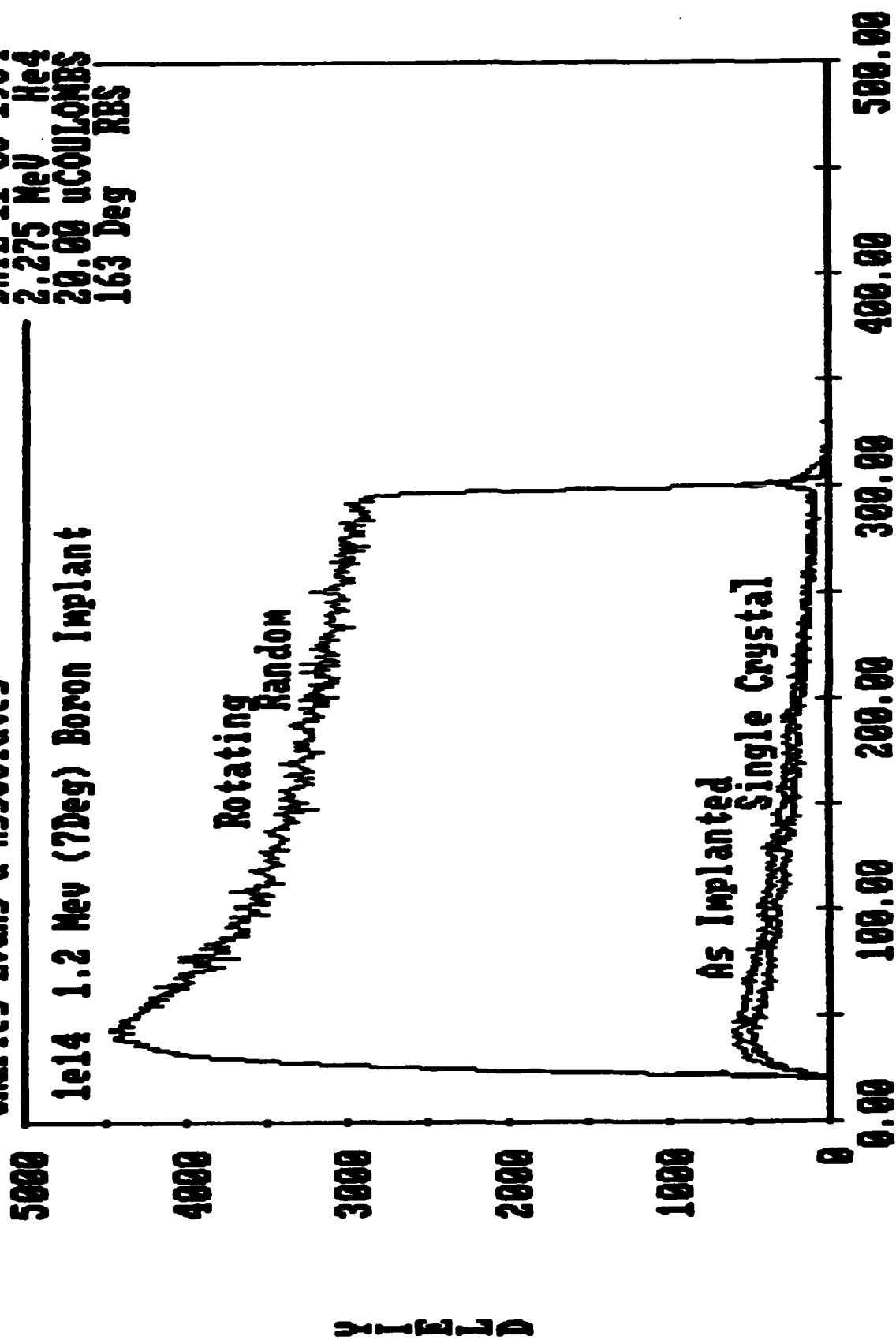


Figure #B 62

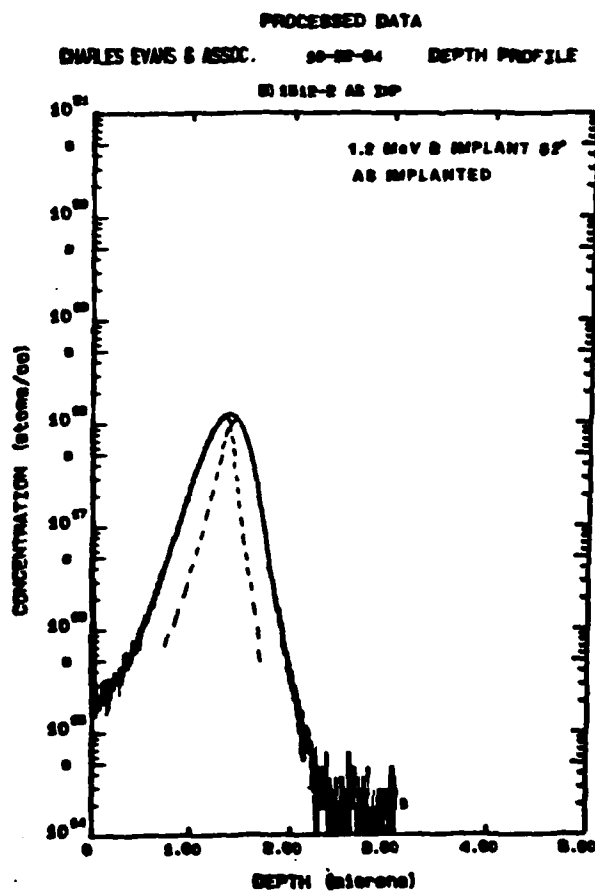
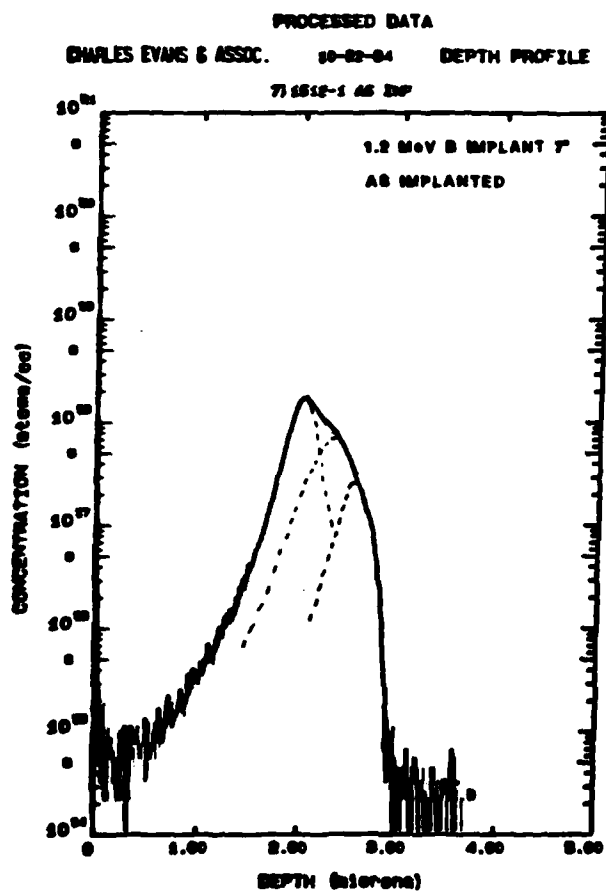
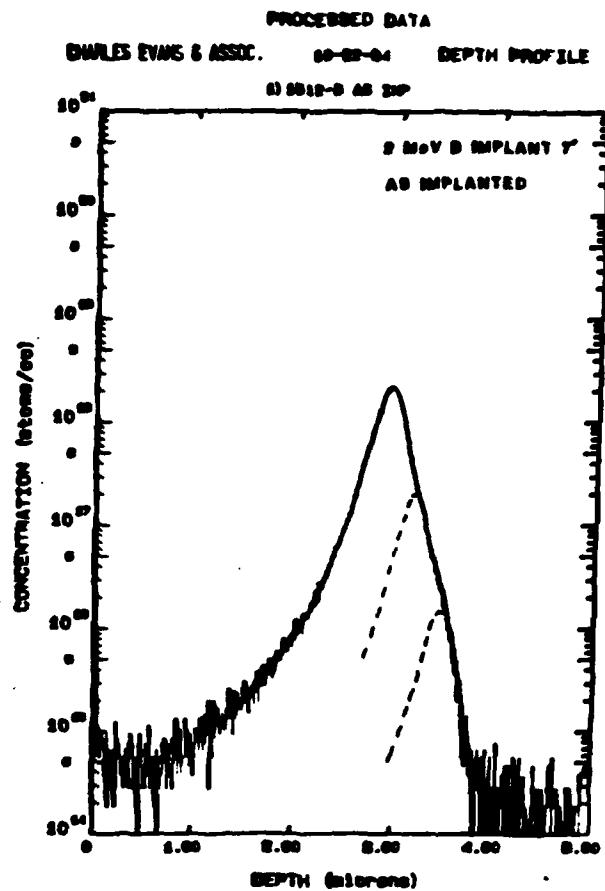
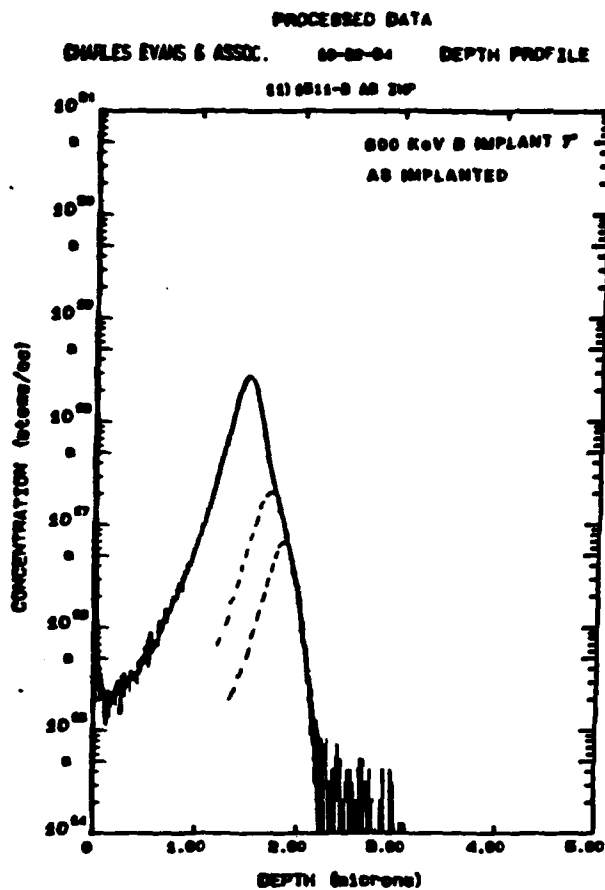
Charles Evans & Associates

DATE 11-06-1984
2.275 MeV He4
20.00 uCOLLOMBS
163 Deg RBS



CHANNEL # GIC TANDETRON

Figure #9



Total Integrated Processed Counts

Sample	As Implanted		Nominal Dose	
		As Implanted	As Implanted	Annealed
800KeV 7° P	#0321-1515-3 8.7E10 6.7E10	7.2	#304-1220-3 4.0E10	8.7E13 4.8E13
1.2MeV 7° P	#0321-1514-1 6.0E10		#304-1218-1 4.8E10	7.2E13 6.8E13
1.2MeV 52° P	#0321-1514-2 3.7E10		#304-1218-2 2.8E10 2.8E10	4.45E13 3.6E13
2.0MeV 7° P	#0321-1517-1 6.8E10 6.2E10	6.0	#304-1218-3 4E10 5E10	7.2E13 5.4E13

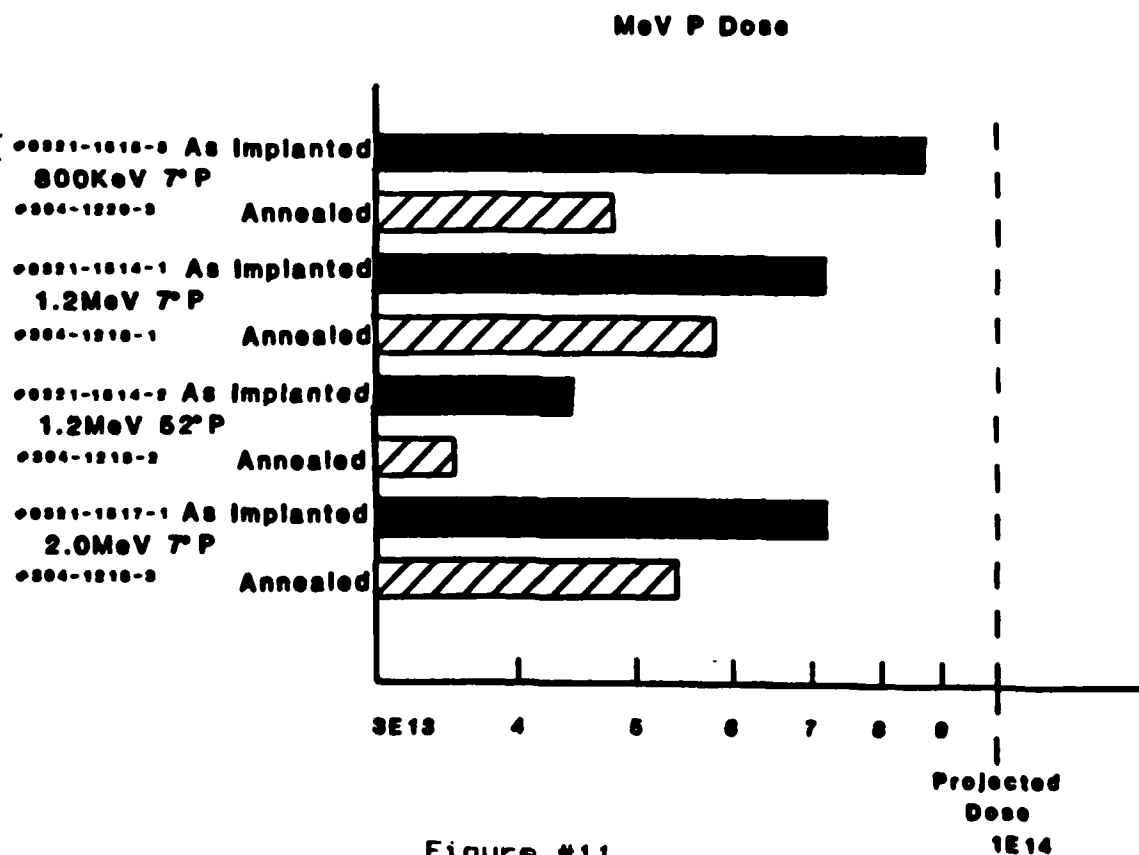


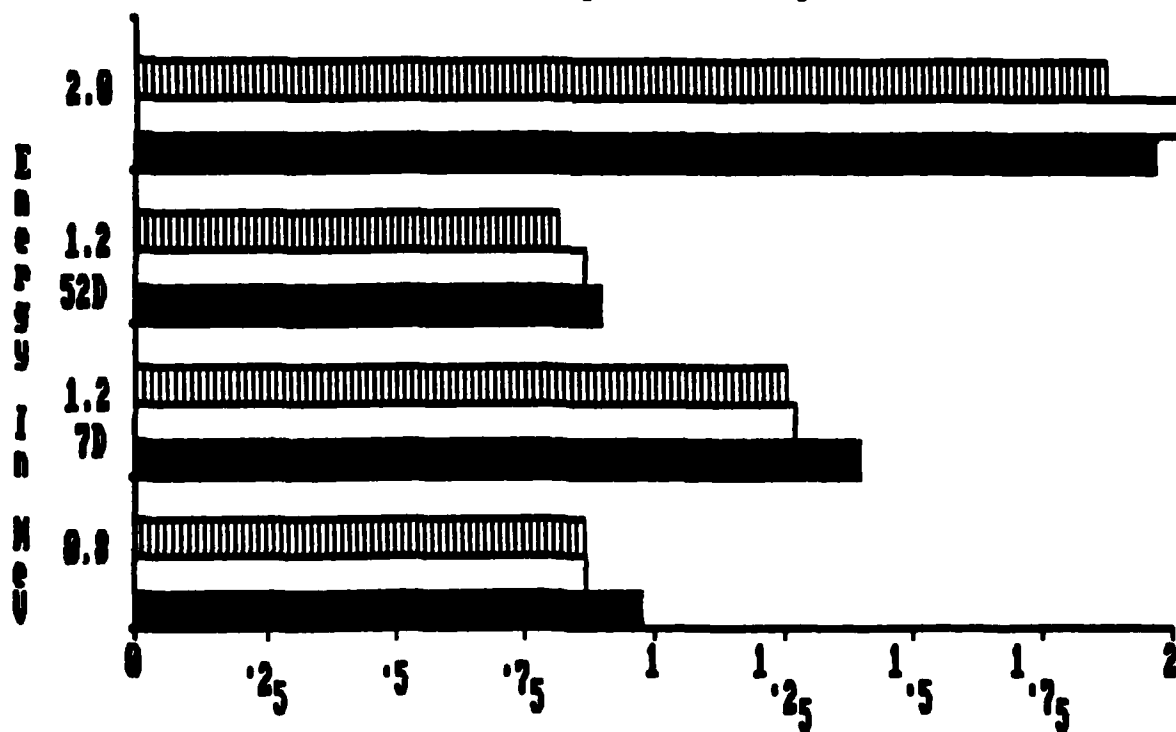
Figure #11

MEV PHOSPHOROUS IMPLANT

MEAN DEPTH IN MICRONS

IMPLANT CONDITIONS	SIMS AS-IMP	SIMS ANNEALED	SRP
0.8 MEV 7 DEGREES	0.98	0.87	0.867
1.2 MEV 7 DEGREES	1.4	1.27	1.25
1.2 MEV 52 DEGREES	0.9	0.865	0.814
2.0 MEV 7 DEGREES	1.97	2.05	1.868

MeV Phosphorous Ion Implant



Mean Depth In Microns
 ■ SIMS AS-IMP □ SIMS ■ SRP

Figure #12

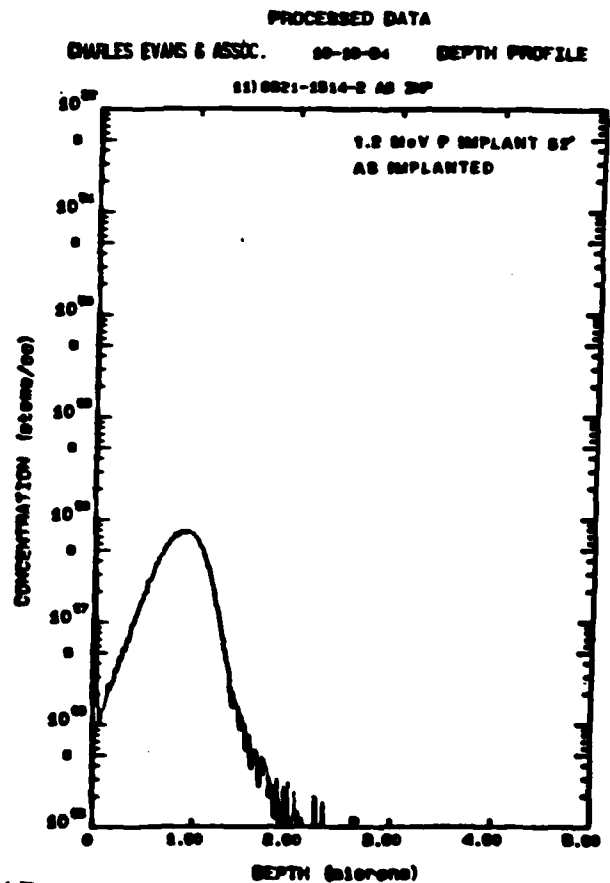
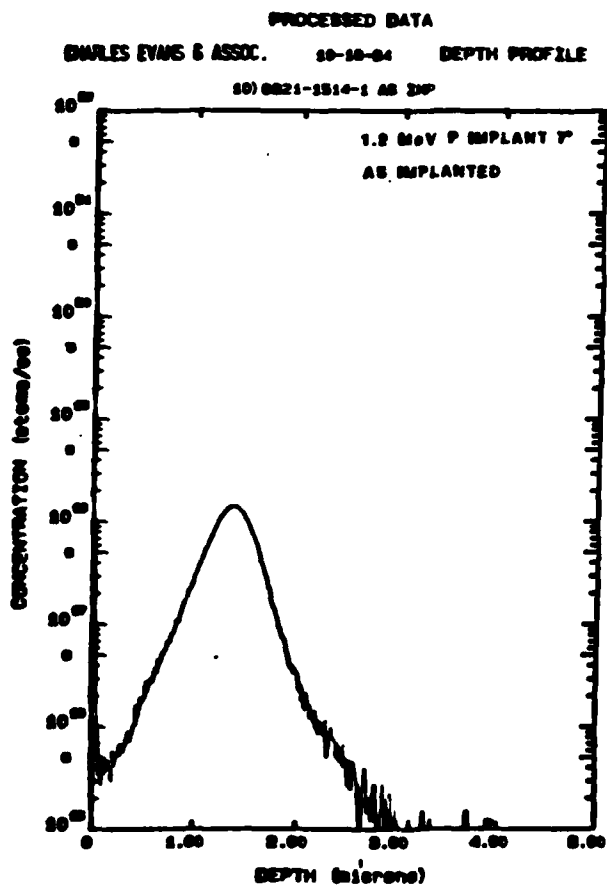
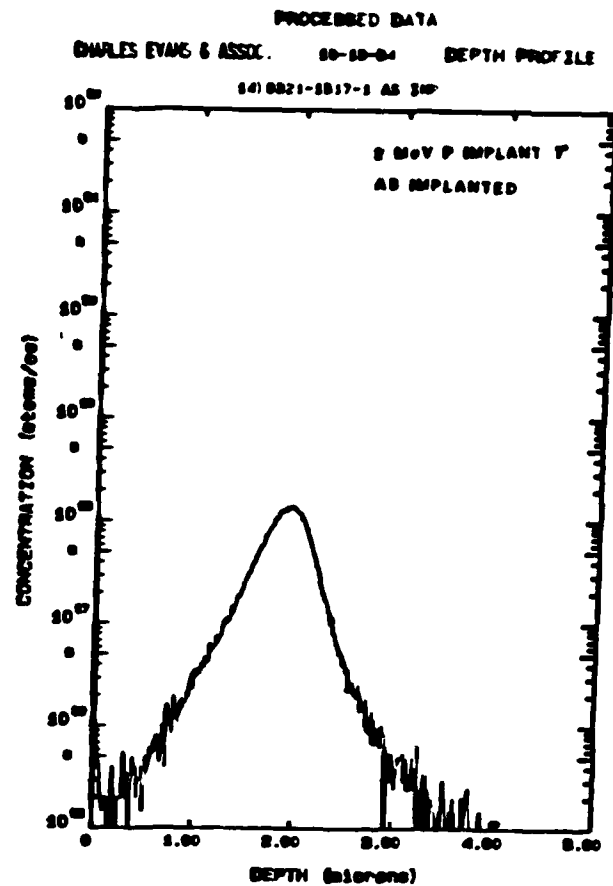
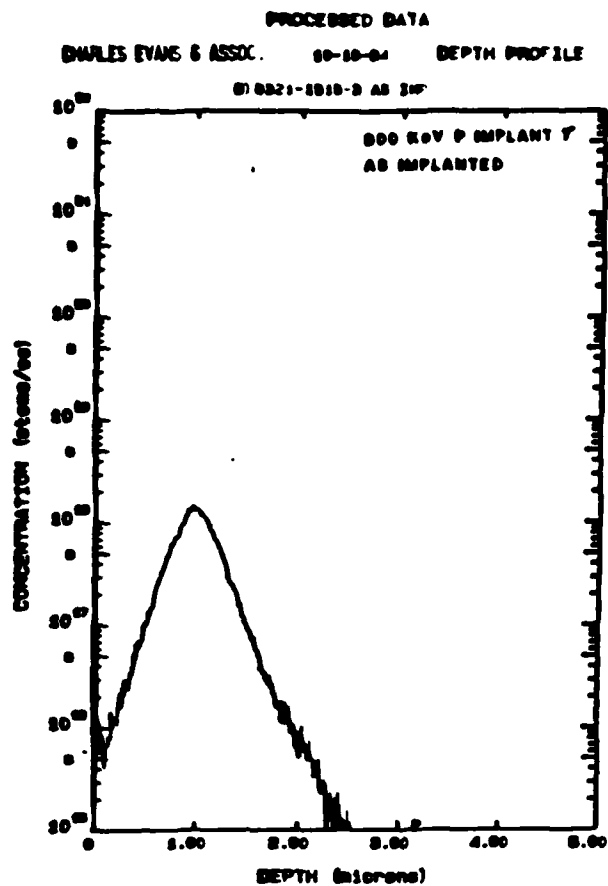


Figure #13

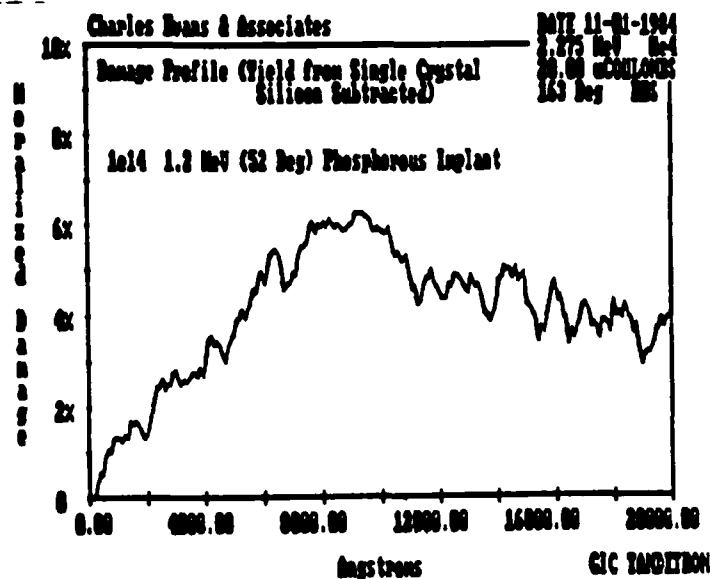
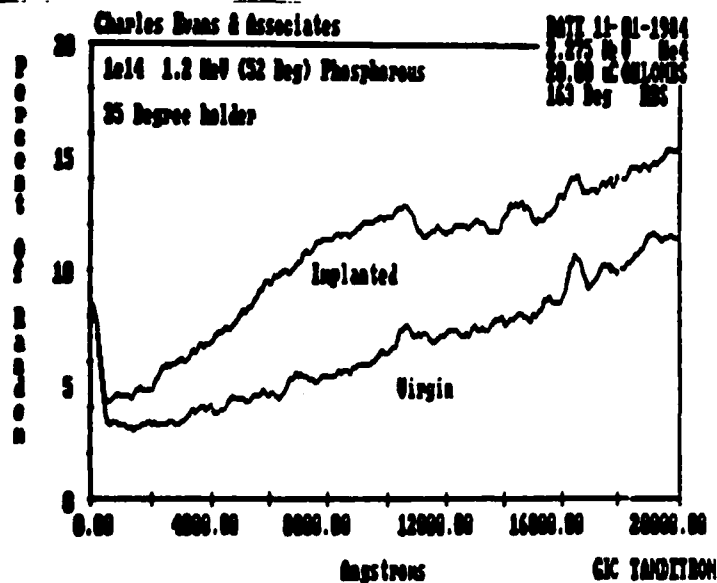
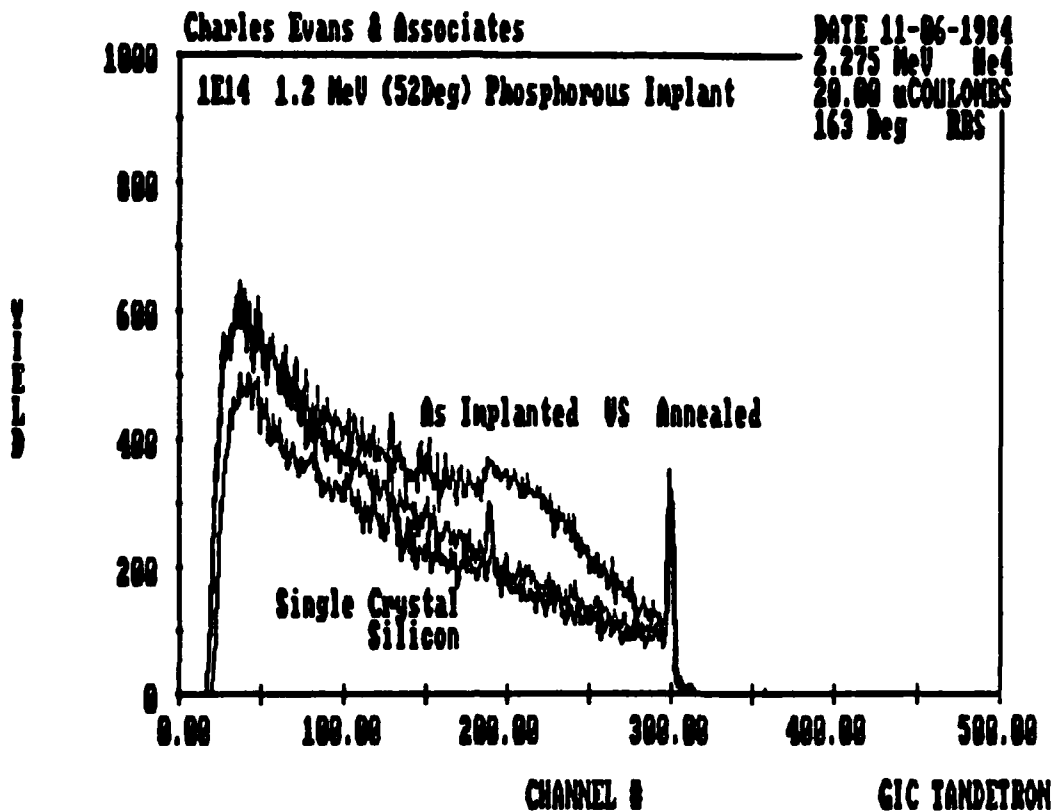


Figure #14